R. & M. No. 3307

MINISTRY OF AVIATION

AERONAUTICAL RESEARCH COUNCIL
REPORTS AND MEMORANDA

Aerodynamic Derivative Measurements on a Wing with a Horn-Balanced Control Surface

By P. R. GUYETT and J. K. CURRAN

LONDON: HER MAJESTY'S STATIONERY OFFICE
1963
PRICE 15s. 6d. NET

Aerodynamic Derivative Measurements on a Wing with a Horn-Balanced Control Surface

By P. R. GUYETT and J. K. CURRAN

COMMUNICATED BY THE DEPUTY CONTROLLER AIRCRAFT (RESEARCH AND DEVELOPMENT), MINISTRY OF AVIATION

*Reports and Memoranda No. 3307**

March, 1961

Summary.

Some oscillatory aerodynamic derivatives for wing pitch and translation, and control-surface rotation have been found from measurements in a low-speed wind tunnel. The wing was a modified cropped delta of biconvex circular-arc section having a small leading-edge radius and fitted with a horn-balanced control surface. The measurements covered a range of control-surface angles with the wing at a mean angle of incidence of 0°.

Control-surface setting influenced the values of all derivatives but the variation was small for angles in the range 0° to 5°. The wing lift and pitching-moment derivatives for wing motion at small control angles were in satisfactory agreement with theoretical results. Derivatives for control-surface rotation at small angles of the control were generally in reasonable agreement with values estimated using theoretical and semi-empirical methods.

1. *Introduction.*

Experiments[1, 2] have shown that it is possible to predict with good accuracy the aerodynamic forces acting at low subsonic speeds on oscillating wings having conventional subsonic-section profiles. Large discrepancies can exist, however, between the corresponding measured and calculated forces arising from control-surface motion[3], where viscous forces play a more significant part, but are inevitably neglected in the theoretical analysis. Viscosity may also be expected to have an important influence on the unsteady forces acting at low speeds on wings with sharp leading edges.

This report describes some oscillatory-force measurements made in a low-speed wind tunnel on a modified cropped delta of biconvex circular-arc section with a small leading-edge radius and fitted with a horn-balanced control surface. With this configuration the problems of predicting aerodynamic forces due to control-surface movement are complicated by the flow through the gap between the wing and the horn. Results were obtained for the range of frequency parameter 0·27 to 1·1, the corresponding Reynolds numbers being between $1{\cdot}4 \times 10^6$ and $0{\cdot}35 \times 10^6$ respectively. Transition wires were fitted to both surfaces of the wing and control horn, at a distance of 25% of the local chord from the leading edge, for all test conditions, and in addition two series of control-surface oscillation tests were made with the wing bare.

* Previously issued as R.A.E. Report No. Structures 263—A.R.C. 23,120.

Measurements were made of the wing lift and pitching moment for rigid wing pitch about a mean angle of incidence of 0° with the control surface set at angles of 0° to 15° to the wing. The results show that both the stiffness and damping derivatives for lift and moment depended upon the control setting. At 0° angle there was reasonable agreement with calculated derivatives.

Measurements were also made of the wing lift and pitching moment and of the control-surface hinge moment for control-surface oscillations about mean angles of 0°, 5° and 10° with the wing held at 0° incidence. The derivatives showed only a small variation in changing the mean control angle from 0° to 5° but generally increased in magnitude at a mean angle of 10°. Results for control-surface amplitudes of 4° and 8° were in fairly close agreement in each case with transition wires fitted. Values of the derivatives for 0° mean angle were in reasonable agreement with theoretical results and with values estimated using a semi-empirical method.

Attempts were made to examine the flow over the wing during oscillatory motion by photographing tufts attached to the wing surface. With the control displaced the film records clearly showed airflow oscillating through the gap opened up at the root of the horn.

2. *Method.*

Aerodynamic derivatives for pitch and normal translation were found by measuring the lift and moment during sustained pitching oscillations about two spanwise axis positions. The lift and pitching moment were determined from the output of a force transducer in a linkage providing the excitation about the axis, and from the output of a force transducer measuring the lift at the axis.

Aerodynamic derivatives for control-surface rotation were found from measurements of the lift and pitching moment on the wing and of the control-surface hinge moment during sustained oscillations of the control with the wing fixed. The wing was fixed by two force transducers which provided restraint in pitch and normal translation and by the wing support frame which provided restraint in roll. A third force transducer was mounted in a driving linkage, normal to the plane of the wing, which oscillated the control surface. Measurements of the reactions at the three force transducers enabled the wing lift and pitching moment to be found, and the control-surface hinge moment was given directly by the force in the linkage.

In each mode of oscillation the reactions of the inertia forces at the force measuring points were reduced by mounting the wing, or the control surface, on a set of earthed springs. The springs were arranged to give a balance between the stiffness and inertia forces at a chosen frequency of oscillation, and this frequency was maintained throughout the tests. Frequency parameter was varied by altering the wind speed.

The method of calculating the required spring stiffnesses and positions has been described in detail in Ref. 1. When a precise balance of stiffness and inertia force is obtained, the forces measured in an oscillation in still air at the chosen frequency arise solely from the still-air aerodynamic damping and the apparatus damping. If the wing is then oscillated in a windstream at the same frequency and amplitude the additional forces measured, which in general are large compared with the still-air forces, give directly the additional aerodynamic forces acting on the wing.

3. *Apparatus.*

3.1. *Wind Tunnel.*

The tests were made in the R.A.E. 5 ft diameter Low-Speed Wind Tunnel. The working section

was closed for these tests by fitting a circular-section tube between the entry nozzle and the safety screen. A fairing was added to the bottom of the tube to give a horizontal flat surface at the model position.

3.2. *Wing and Support.*

The half-span model wing was mounted vertically in the wind tunnel and was supported through a slot in the fairing at the bottom of the circular tube. To reduce the air flow through this slot and around the wing root a metal plate was fixed to the wing and oscillated with it. In addition wooden strips were fitted on the fairing around the metal plate to form a shallow well. Fig. 2 shows the position of the model in the tunnel. The horizontal flat surfaces normal to the wing at its root were considered to act as a reflector plate to simulate symmetrical aerodynamic loading.

Dimensions of the wing and control surface are given in Fig. 1. The wing was of modified cropped delta planform. Over the inboard wing the leading edge was swept back 38°, and over the horn the leading edge was swept back 65°. Inboard of the horn the control-surface chord was constant and equal to 27% of the wing mean chord. The wing geometric aspect ratio was 1·04, equivalent to a full-span aspect ratio of 2·08. The wing section was a biconvex circular arc with a blunt trailing edge of thickness equal to 0·4% of the chord, and with a rounded leading edge of radius approximately 0·6% of the chord. The thickness/chord ratio was 0·04 for the inboard wing, and increased to 0·08 at the tip.

The main wing surface was made of sheet steel welded to spanwise steel webs and screwed and riveted to solid steel members which formed the wing leading edge and root. The control surface was moulded in Durestos, and attached to the wing by two plain bearings at the root of the wing and the horn. Three Duralumin brackets were bolted to the wing root through the Duralumin reflector plate. A steel channel was bolted into the front or rear bracket and carried a cross-spring bearing unit forming the pitching axis. The cross-spring bearing was bolted to a rectangular welded frame which in turn was attached to a further cross-spring bearing unit bolted to a vertical member in a heavy base frame. Fig. 3 shows the arrangement for wing pitch about the forward axis. A force transducer was connected between the base and the rectangular frame close to the pitching axis. The output of this transducer was thus proportional to the lift force acting on the axis.

The driving rod used to excite the pitching modes of oscillation was connected to the central root bracket. Duralumin angles bridging the three brackets provided an attachment for the springs required for balancing the inertia force. For the pitching-oscillation tests the control surface was locked to the rear bracket by two studs at the root of the control surface which passed through slots in the reflector plate. For the control-surface oscillations with wing fixed, the wing was supported as shown in Fig. 3 but with a second force transducer connected between the rear bracket and an adjacent rigid structure. The two force transducers thus measured the lift and pitching moment acting on the fixed wing including the reaction at the control-surface hinge line. A metal plate was bolted to the control-surface studs and the driving linkage was coupled to it between the rear brackets. Springs were connected between the plate and earth and adjusted to cancel the inertia loads on the control-surface hinge and the direct inertia load in the exciter transducer.

3.3. *Excitation.*

In each mode the oscillation was maintained by forcing from a swash-plate exciter (Fig. 2). The angle of tilt of the swash plate could be varied smoothly to alter the amplitude of oscillation of a plunger projecting from the body of the exciter. Sinusoidal forcing from the plunger was transmitted

through a spring and linkage to a driving rod coupled to the wing or control surface. Cross-spring bearings were used throughout to minimise the apparatus damping.

3.4. *Frequency Measurement.*

Balance between the spring and inertia forces occurs only at the chosen frequency, and thus to avoid errors in the force measurements this frequency must be accurately maintained.

Frequency was measured at 10 second intervals during the test and corrected by manually adjusting the speed of the exciter motor. An electronic counter[4] measured the frequency to an accuracy of about $\pm 0{\cdot}05\%$ and generally it was maintained to within $\pm 0{\cdot}1\%$ of the chosen value.

3.5. *Force Measurement and Recording.*

Applied forces normal to the mean plate of the wing were measured by force transducers in the driving linkage and at the wing root. (Fig. 2 and Section 2.)

A force transducer is shown in Fig. 4. The ends of two beryllium copper strips were attached to a channel section forming the body of the unit, and these strips were placed in tension by tightening two bolts in a block connecting their centres. Load applied to the connector then caused an increase in tension in one strip and a decrease in the other. Four wire-resistance strain gauges cemented to the strips were connected to form a Wheatstone bridge sensitive to loading in the axial direction.

Output from the galvanometer arm of the Wheatstone bridge was supplied to a pair of brushes bearing at 180° on a two-segment commutator mounted on the shaft of the exciter and rotating at the wing oscillation frequency. Each of the two commutator segments was coupled to an outer slip ring which was connected to the galvanometer. The transducer output was thus reversed in direction after each half cycle of oscillation by the commutator to produce a signal having a mean d.c. level which was measured by the galvanometer. The transducer output could also be switched to a second pair of brushes at 90° to the first pair. Fig. 5 indicates the arrangement of the commutator and Fig. 6 the form of the resultant signals. It may be shown that for a sinusoidal input signal the two galvanometer readings are:

Switched to 1st pair of brushes,

$$\text{response} = -\frac{2}{\pi} S_0 \cos\psi,$$

Switched to 2nd pair of brushes,

$$\text{response} = \frac{2}{\pi} S_0 \sin\psi.$$

From these two readings the amplitudes of the transducer outputs and their phase relationships to the commutator were found. The phase angle between the commutator rotation and the wing displacement depended upon the wing load since the exciting force was applied through a spring. To establish this angle a strain-gauged cantilever strip was connected to the wing or control surface and its output also supplied to the commutator and measured by the galvanometer. The cantilever produced a signal in phase with the wing displacement and thus from the two sets of measurements the components of the transducer output in phase and in quadrature with the wing displacement were found.

4. *Test Procedure.*

In each mode the reactions of the inertia forces at the force transducers were reduced by oscillating the wing or control surface against earthed springs as described in Section 2. Generally a precise balance of inertia and stiffness force was not achieved but instead spring stiffnesses and positions

were found for which the resulting reactions were well below the level of the aerodynamic forces. These residual forces, in phase with the motion, and the accompanying quadrature forces required to overcome the structural and aerodynamic forces were then measured in still air at the chosen frequency and amplitude of oscillation. Measurements were then made at the same frequency and amplitude at wind speeds between 40 ft/sec and 160 ft/sec. Following the wind-on tests a further set of measurements was made in still air. The aerodynamic forces due to the windstream were taken to be the difference between the wind-on and still-air force measurements.

The in-phase forces found in this way correspond to the aerodynamic forces due to displacement alone, since the virtual-inertia forces, which are present both with the wind on and in still air, are excluded by the subtraction. Similarly the derived forces in quadrature with the wing motion do not include the still-air aerodynamic damping.

The force transducers were calibrated dynamically by attaching masses to the wing or control surface and measuring the additional outputs in oscillations at the test frequency and amplitudes.

Static aerodynamic force and moment derivatives were found by disconnecting the main springs and measuring the change of force at each transducer over a range of wing incidence or control-surface angle at a fixed wind speed. Corrections were applied for the forces arising from the stiffness of the cross-spring bearings.

Transition wires were fitted to both surfaces of the wing and horn, at a distance of 25% of the local chord from the leading edge, in all tests except two series of control-surface oscillations at a mean angle of 0°.

5. *Presentation of Results.*

The results are given as overall derivatives and as equivalent constant-strip derivatives*. The strip derivatives are referred to the wing local leading edge and thus apply strictly only to motion in the two experimental modes, since the displacement co-ordinates of translation and pitch about the strip leading edge are not independent for rigid wing modes. In the chosen form the derivatives may, however, be treated in the same way as two-dimensional leading-edge derivatives† in evaluating approximate aerodynamic force coefficients for general wing modes.

The lift, moment about the leading edge, and the hinge moment‡ acting on a typical chordwise strip are therefore given by—

$$L = \rho V^2 c dy \left\{ (l_z + ivl_{\dot{z}}) \frac{z}{c} + (l_\alpha + ivl_{\dot{\alpha}})\alpha + (l_\beta + ivl_{\dot{\beta}})\beta \right\},$$

$$M = \rho V^2 c^2 dy \left\{ (m_z + ivm_{\dot{z}}) \frac{z}{c} + (m_\alpha + ivm_{\dot{\alpha}})\alpha + (m_\beta + ivm_{\dot{\beta}})\beta \right\},$$

$$H = \rho V^2 c^2 dy \{ (h_\beta + ivh_{\dot{\beta}})\beta \},$$

where l_z, $l_{\dot{z}}$, . . . , h_β, $h_{\dot{\beta}}$ are equivalent constant-strip derivatives appropriate to the wing mean frequency parameter, ν_m.

---

* Equivalent constant strip derivatives are defined as derivatives which are chosen to be independent of spanwise position but which when integrated over the wing in the appropriate mode give the correct generalised forces; the values of the derivatives depend upon the planform, the modes of oscillation, the position of the reference axis, the mean frequency parameter and the Mach number.

† *See*, for example, the method given by Templeton[5].

‡ Hinge moments arising from wing motion in normal translation and pitch were not measured, and are therefore omitted from the hinge-moment expression.

Now,

$$\nu = \frac{c}{c_m}\nu_m$$

$$z = z' + (c' - c)\alpha$$

$$c_m = 1{\cdot}396 \text{ ft}$$

$$c' = 2{\cdot}056 \text{ ft}$$

$$s = 1{\cdot}450 \text{ ft}$$

and it may be shown that,

$$\int_0^1 c\,d\eta = 0{\cdot}6789c',$$

$$\int_0^1 c^2 d\eta = 0{\cdot}5115c'^2,$$

$$\int_0^1 c^3 d\eta = 0{\cdot}4088c'^3.$$

By integrating the lift, moment, and hinge moment over the wing from root to tip, for rigid wing motion in z', α and β the following results may be obtained:

$$\frac{\text{Lift}}{\rho V^2 s c'} = l_z \frac{z'}{c'} + 0{\cdot}3211 l_z\alpha + 0{\cdot}6789 l_\alpha\alpha + i\nu_m \frac{c'}{c_m}(0{\cdot}6789 l_{\dot z}\frac{z'}{c'} + 0{\cdot}1674 l_{\dot z}\alpha +$$

$$+ 0{\cdot}5115 l_{\dot\alpha}\alpha) + 0{\cdot}6789 l_\beta\beta + i\nu_m \frac{c'}{c_m} 0{\cdot}5115 l_{\dot\beta}\beta,$$

$$\frac{\text{Moment about root leading edge}}{\rho V^2 s c'^2} = -0{\cdot}3211 l_z \frac{z'}{c'} + 0{\cdot}6789 m_z \frac{z'}{c'} - 0{\cdot}1537 l_z\alpha +$$

$$+ 0{\cdot}1674 m_z\alpha - 0{\cdot}1674 l_\alpha\alpha + 0{\cdot}5115 m_\alpha\alpha +$$

$$+ i\nu_m \frac{c'}{c_m}\Big(-0{\cdot}1674 l_{\dot z}\frac{z'}{c'} + 0{\cdot}5115 m_{\dot z}\frac{z'}{c'} -$$

$$- 0{\cdot}0647 l_{\dot z}\alpha + 0{\cdot}1027 m_{\dot z}\alpha - 0{\cdot}1027 l_{\dot\alpha}\alpha +$$

$$+ 0{\cdot}4088 m_{\dot\alpha}\alpha\Big) + 0{\cdot}5115 m_{\dot\beta}\beta - 0{\cdot}1674 l_\beta\beta +$$

$$+ i\nu_m \frac{c'}{c_m}(0{\cdot}4088 m_{\dot\beta}\beta - 0{\cdot}1027 l_{\dot\beta}\beta),$$

$$\frac{\text{Hinge moment}}{\rho V^2 s c'^2} = 0{\cdot}5115 h_\beta\beta + i\nu_m \frac{c'}{c_m} 0{\cdot}4088 h_{\dot\beta}\beta.$$

5.1. *Pitching about the Forward Axis with the Control Locked to the Wing.*

$$\frac{z'}{c'} = -0{\cdot}302\alpha, \quad \beta = 0.$$

Hence,

$$\frac{\text{Lift}}{\rho V^2 sc'\alpha} = 0{\cdot}6789l_\alpha + 0{\cdot}0192l_z + iv_m\frac{c'}{c_m}(-0{\cdot}0376l_{\dot z} + 0{\cdot}5115l_{\dot\alpha})$$

$$= (l_\theta)_f + iv_m\frac{c'}{c_m}(l_{\dot\theta})_f, \text{ say.}$$

$$\frac{\text{Pitching moment about root leading edge}}{\rho V^2 sc'^2\alpha} = -0{\cdot}05675l_z - 0{\cdot}1674l_\alpha - 0{\cdot}03763m_z +$$
$$+ 0{\cdot}5115m_\alpha + iv_m\frac{c'}{c_m}(-0{\cdot}0141l_{\dot z} - 0{\cdot}1027l_{\dot\alpha} - 0{\cdot}0518m_{\dot z} + 0{\cdot}4088m_{\dot\alpha})$$
$$= (m_\theta)_f + iv_m\frac{c'}{c_m}(m_{\dot\theta})_f, \text{ say.}$$

The measured overall derivatives $(l_\theta)_f$, $(l_{\dot\theta})_f$, $(m_\theta)_f$ and $(m_{\dot\theta})_f$ are plotted against mean frequency parameter in Figs. 9 and 10.

5.2. *Pitching about the Rear Axis with the Control Locked to the Wing.*

$$\frac{z'}{c'} = -0{\cdot}7073\alpha, \quad \beta = 0.$$

Hence,

$$\frac{\text{Lift}}{\rho V^2 sc'\alpha} = 0{\cdot}6789l_\alpha - 0{\cdot}3862l_z + iv_m\frac{c'}{c_m}(-0{\cdot}3128l_{\dot z} + 0{\cdot}5115l_{\dot\alpha})$$

$$= (l_\theta)_r + iv_m\frac{c'}{c_m}(l_{\dot\theta})_r, \text{ say.}$$

$$\frac{\text{Pitching moment about root leading edge}}{\rho V^2 sc'^2\alpha} = 0{\cdot}0734l_z - 0{\cdot}1674l_\alpha - 0{\cdot}3128m_z +$$
$$+ 0{\cdot}5115m_\alpha + iv_m\frac{c'}{c_m}(0{\cdot}0537l_{\dot z} - 0{\cdot}1027l_{\dot\alpha} - 0{\cdot}2591m_{\dot z} + 0{\cdot}4088m_{\dot\alpha})$$
$$= (m_\theta)_r + iv_m\frac{c'}{c_m}(m_{\dot\theta})_r, \text{ say.}$$

The measured overall derivatives $(l_\theta)_r$, $(l_{\dot\theta})_r$, $(m_\theta)_r$ and $(m_{\dot\theta})_r$ are plotted against mean frequency parameter in Figs. 11 and 12.

5.3. *Control Oscillation with Wing Held.*

$$z' = \alpha = 0.$$

Hence

$$\frac{\text{Lift}}{\rho V^2 sc'\beta} = 0{\cdot}6789l_\beta + iv_m\frac{c'}{c_m}0{\cdot}5115l_{\dot\beta}$$

$$\frac{\text{Pitching moment about root leading edge}}{\rho V^2 sc'^2\beta} = 0{\cdot}5115m_\beta - 0{\cdot}1674l_\beta +$$
$$+ iv_m\frac{c'}{c_m}(0{\cdot}4088m_{\dot\beta} - 0{\cdot}1027l_{\dot\beta})$$

$$\frac{\text{Hinge moment}}{\rho V^2 sc'^2\beta} = 0{\cdot}5115h_\beta + iv_m\frac{c'}{c_m}0{\cdot}4088h_{\dot\beta}.$$

The measured values of these derivatives are plotted against mean frequency parameter in Figs. 17 to 25.

5.4. *Equivalent Constant-Strip Derivatives.*

From the curves in Figs. 9 to 12 the individual derivatives l_z, $l_{\dot{z}}$, . . . , $m_{\dot{\alpha}}$ have been found and are plotted against mean frequency parameter in Figs. 13 to 16.

Similarly the derivatives m_β and $m_{\dot{\beta}}$ have been found from the results given in Figs. 17 and 18, 20 and 21, 23 and 24 and are plotted against mean frequency parameter in Figs. 26 to 28.

6. *Discussion of Results and Comparison with Theory.*

6.1. *Corrections for Rig Deformation.*

In oscillations in still air the amount of deformation was negligible, but with the wind on deformation occurred consisting primarily of twist of the rectangular root frame due to the aerodynamic rolling moment. Since any change of mode alters the balance between the inertia and spring reaction forces, as well as introducing additional aerodynamic forces, calculations were made for each configuration at the maximum test speed to assess these effects. A sample calculation is described in the Appendix. The average correction to the values of the overall derivatives was approximately 1% with a maximum of 3·3%; as these corrections are small they have not been applied to the results.

6.2. *Corrections for Wind-Tunnel Wall Constraint.*

Static wind-tunnel corrections for the test configuration, calculated from the results of Ref. 1, indicate that the measured stiffness derivatives at low frequency parameters are about $3\frac{1}{2}$% higher than the free-stream values. From the existing results[6, 7] for oscillating wings in closed wind tunnels the corrections to the stiffness derivatives are greatest at low frequency parameter and the corrections to damping derivatives are small. Thus the measured derivatives are probably subject to only small errors from wall constraint, and are therefore given without any corrections applied.

6.3. *Pitching Oscillations about the Forward Axis.*

Wing lift and moment derivatives for each setting of the control surface are plotted against frequency parameter in Figs. 9 and 10. Derivatives which have been calculated by Bristol Aircraft Ltd., using the Multhopp-Garner method are given for comparison. Also shown are some values obtained by interpolation from results calculated by Lehrian[8]; these apply to a cropped delta of the same aspect ratio as the test wing.

The derivatives for 0° relative angle between control and wing show little variation with frequency parameter, and are in reasonable agreement with the theoretical values. Increasing the aileron-wing angle in the range 0° to 10° generally increased the magnitude of the stiffness lift and moment derivatives. A further increase of angle to 15° reduced their magnitude but they remained above the values for 0° angle. The trends of change of the damping-force derivatives are less clear. At 5° angle the derivatives are rather larger in magnitude than at 0°; at 10° and 15° they are markedly dependent upon frequency parameter.

Altering the control setting at the constant test-wing mean incidence of 0° produced steady loads on the wing, and thus may be regarded as equivalent in some respects to changing the wing mean incidence. Scruton[2] has measured the effect of mean wing incidence on the corresponding oscillatory derivatives for a cropped delta wing. His results also show increases in the magnitude of stiffness force derivatives for small increases of incidence and reductions at larger incidence, and indicate that the damping-force derivatives varied with mean incidence and frequency parameter at high incidence.

Some cine-film camera records were taken of the behaviour of tufts fixed to the wing surface to obtain an indication of the flow conditions during steady and oscillatory wing motion. The tufts moved regularly with wing displacement at the test frequency and it is believed that they provided a fairly accurate qualitative picture of the flow directions. With the control deflected the records clearly showed flow oscillating through the gap opened up between the horn and the wing. At the largest angles the tufts indicated breakaway over the suction surface of the control between the root of the horn and the wing root, with the flow attached over part of the surface of the horn itself. Fig. 8 shows a sequence of camera pictures of the outer wing and horn covering rather more than one-quarter of a cycle of wing oscillation. The control surface was fixed to the wing at an angle of $7\frac{1}{2}°$ and the wing was oscillated through $\pm$ 3° about a mean incidence of 0°. In frame 1 the tufts all lie in the streamwise direction (with the exception of the third tuft at the horn root which had become fixed at the transition wire). As the wing was displaced the tufts at the front of the horn at its root curled into the gap, and the tuft at the tip leading edge of the horn was drawn over the tip. In frame 3 the tuft on the horn at the rear of the gap is also curled into the gap and the second tuft from the tip is drawn over the leading edge. Subsequent pictures show the tufts on the wing near the gap curving towards the gap.

The existence of an oscillatory flow through the horn gap is not unexpected and could give rise to the measured effects of frequency parameter upon the magnitude of the derivatives. In the tests the phase angles between the resultant oscillatory force and displacement vectors were between 10° and 20°, and thus a small change of phase angle, which could be produced by the gap and depend upon the frequency parameter, would have a greater influence upon the damping forces than the stiffness forces. An explanation can therefore be found for the measured results, but it is considered extremely unlikely that they can be predicted in detail.

The generally good agreement between the two sets of theoretical results suggests that the derivatives do not vary greatly with frequency parameter or depend critically upon the planform.

6.4. *Pitching Oscillations about the Rear Axis.*

The measured results are plotted in Figs. 11 and 12 together with the theoretical values.

The stiffness derivatives for 0° aileron angle are practically independent of frequency parameter over the test range; the corresponding damping derivatives increase slightly with frequency parameter. Both sets of derivatives are in reasonable agreement with the theoretical values.

The stiffness derivatives show the same trend of change with aileron angle that occurred at the forward axis position, and again the damping derivatives show only a small variation with aileron angle in the range 0° to 5°.

6.5. *Wing Lift and Moment Derivatives.*

From the results in Figs. 9 to 12 and the relations in Section 5 equivalent constant-strip derivatives referred to the local leading edge have been found and are given in Figs. 13 to 16.

The rates of change of the pitching derivatives (Figs. 15 and 16) with aileron angle are generally smaller than the corresponding changes of the translation derivatives (Figs. 13 and 14).

6.6. *Wing Lift and Moment and Aileron Hinge Moment due to Aileron Rotation.*

Results for a mean aileron angle of 0° are given in Figs. 17, 18, 19 and 26. The derivatives l_β and m_β are largely independent of frequency parameter, aileron amplitude and the transition point

within the ranges considered. The corresponding damping derivatives $l_{\dot{\beta}}$ and $m_{\dot{\beta}}$ show some dependence upon amplitude with the transition fixed and a marked dependence upon amplitude for free transition. In both conditions the values of the damping derivatives fall as the frequency parameter is reduced below 0·4. The hinge-moment damping derivative $h_{\dot{\beta}}$ is practically independent of frequency parameter, amplitude and the transition point. The stiffness derivative h_{β} also shows only a small variation with frequency parameter for transition fixed but depends to some extent upon amplitude. For free transition h_{β} varies with both amplitude and frequency parameter.

Figs. 20, 21, 22 and 27 show the results for a mean aileron angle of 5° and fixed transition. In the test range, the derivatives vary only slightly with amplitude although the variation is more marked on the stiffness derivatives than on the damping derivatives. In general the values and trends agree fairly well with those for 0° mean aileron angle. An exception is h_{β} which decreases with increasing frequency parameter.

At 10° mean aileron angle (Figs. 23 to 25 and 28) the derivatives are larger in magnitude than at 0° and 5°, and $l_{\dot{\beta}}$ and $m_{\dot{\beta}}$ in particular show more variation with frequency parameter. Again the changes with amplitude are fairly small.

Film records of the movement of tufts fitted to the wing and aileron indicated that there was airflow through the gap between the front of the horn and the wing during the aileron oscillations. This flow was apparently small at a mean aileron setting of 0°.

The lift and pitching-moment derivatives calculated by the Multhopp-Garner method are in generally good agreement with the measured results. The corresponding damping hinge-moment derivatives are also in reasonable agreement for the smaller control settings. There is, however, a large discrepancy between the calculated and measured stiffness hinge moments, where the experimental results indicate that the derivative is sensitive to the conditions in the boundary layer.

It is of interest to compare the measured derivatives with results calculated on a simple theoretical basis. Figs. 29 to 31 show the derivatives for a mean aileron angle of 0° and transition fixed together with some calculated values. In finding each set of calculated derivatives the aerodynamic forces on the horn were assumed to be given by slender-body theory—the horn being treated as half of a full-span cropped delta. To obtain the wing lift and moment results in Figs. 29 and 30 the wing inboard of the horn was divided into four chordwise sections of equal width and forces appropriate to the local frequency parameter and chord ratio were found for each section using first two-dimensional[9] and then finite aspect-ratio wing derivatives. The finite wing derivatives used were equivalent constant strip derivatives for a rectangular wing of aspect ratio 2 (practically equal to the test-wing aspect ratio) with a full-span control surface, which were calculated by Minhinnick from work by Lawrence and Gerber[10]. The measured values of l_{β} and $l_{\dot{\beta}}$ are in fairly good agreement with the results calculated using finite aspect-ratio theory for the inner wing but are in poor agreement with the corresponding results using two-dimensional theory. The measured damping derivative, however, shows the same trend at low-frequency parameters as the results using two-dimensional theory. Fig. 30 shows that the measured values for the stiffness moment derivative m_{β} are rather larger than the calculated values using finite-wing theory, which indicates that this method of calculation, in addition to slightly underestimating the magnitude of the lift in phase with the motion also underestimates the distance of its mean centre of pressure from the wing leading edge. Curves of the damping moment derivative are similar in trend to those for the damping lift derivative. Values for the hinge-moment derivatives are compared in Fig. 31. Forces on the control surface inboard of the horn were found by dividing the inboard wing into sections as before and using

factored and unfactored two-dimensional hinge-moment derivatives. The factor used was 0·6 which was found by Wight[3] to be approximately the ratio of the measured to the theoretical value of the direct aileron derivatives from tests on a 15% thick wing with a 20% chord aileron in two-dimensional flow. Applying this factor increases the resultant value of h_β since the in-phase moment from the horn is larger than and opposes the stabilising moment from the inboard control. The results show that a factor of value 0·8 would give excellent agreement between the measured and estimated derivatives, and since the test wing is thinner and has a smaller trailing-edge angle (about 8°) than the wing tested by Wight (15°) a higher value for the factor is probably appropriate. For the damping hinge moment better agreement would be obtained if the value of the factor was smaller than 0·6. There is some evidence[3] that $h_{\dot\beta}$ is less sensitive to trailing-edge angle than h_β and thus there is no reason why the values of the factors should be identical.

In general, the derivatives calculated using the semi-empirical methods described are in reasonable agreement with the measured values. The order of agreement is better than that obtained using the theoretical method which does not take into account wing thickness and flow through the horn-wing gap. It is doubtful if the corresponding forces for large mean aileron angles can be predicted satisfactorily.

7. *Conclusions.*

The results of a series of measurements of oscillatory aerodynamic derivatives at low wind speeds on a modified cropped delta having a biconvex circular-arc section with a small leading-edge radius, and fitted with a horn-balanced control surface, show that:

(i) The wing lift and pitching-moment derivatives for wing pitch and translation about wing mean angles of incidence of 0° depend upon the setting of the control surface. For 0° angle between wing and control the lift and moment stiffness derivatives are practically independent of frequency parameter in the test range 0·3 to 0·7, and the corresponding variation in the damping derivatives is small. The values agree fairly well with theoretical results. As the control angle is increased from 0° to 10° the stiffness derivatives increase in magnitude but fall with a further increase to 15°. The damping derivatives change to a small extent as the control-surface angle is increased from 0° to 5° but at larger angles vary considerably with angle and frequency parameter.

(ii) With transition wires fitted to the wing and control horn at 25% of the local chord aft of the leading edge, and with the wing held at 0° incidence, the lift, pitch and hinge-moment stiffness derivatives for control oscillations about a mean angle of 0° are largely independent of frequency parameter in the test range 0·3 to 1·1. The corresponding hinge-moment damping derivative is also independent of frequency parameter but the values of the lift and pitching-moment damping derivatives fall as frequency parameter is reduced below 0·4. All derivatives show only small changes in value as the mean angle increases to 5° but have larger values at 10° mean angle. Measurements at control-surface amplitudes of approximately 4° and 8° gave generally similar results in all cases. The derivatives for control-surface motion at small angles of the control are in reasonable agreement with values calculated using theoretical and semi-empirical methods. A limited series of tests with natural transition indicate that certain of the derivatives are sensitive to oscillation amplitude and frequency parameter in this condition.

NOTATION

S_0	Amplitude of transducer output
ψ	Phase angle between commutator rotation and wing oscillation
c	Local wing chord
c'	Wing root chord
c_m	Wing mean chord $\left(= \frac{\text{wing area}}{\text{semi-span}}\right)$
s	Wing semi-span
y	Distance of chordwise strip from root
dy	Width of chordwise strip
η	Non-dimensional spanwise co-ordinate $\left(= \frac{y}{s}\right)$
α	Angle of pitch, positive nose up (radians)
z	Displacement of leading edge of chordwise strip, positive downwards
z'	Displacement of wing leading edge at the root, positive downwards
β	Control-surface rotation, positive nose up (radians)
L	Lift acting on chordwise strip, width dy
M	Moment acting about leading edge of strip width dy, positive direction nose up
H	Hinge moment acting on strip width dy, positive direction control surface nose up
ω	Circular frequency of oscillation
V	Wind speed
ρ	Air density
ν	Local frequency parameter $\left(= \frac{\omega c}{V}\right)$
ν_m	Mean frequency parameter $\left(= \frac{\omega c_m}{V}\right)$
l_z, l_α, l_β	Non-dimensional, equivalent constant strip, lift stiffness derivatives for motion in normal translation, pitch, control-surface rotation, respectively
$l_{\dot{z}}$, $l_{\dot{\alpha}}$, $l_{\dot{\beta}}$	Non-dimensional, equivalent constant strip, lift damping derivatives for motion in normal translation, pitch, control-surface rotation, respectively

m_z, m_α, m_β Non-dimensional, equivalent constant strip, pitching-moment stiffness derivatives for motion in normal translation, pitch, control-surface rotation, respectively

$m_{\dot{z}}$, $m_{\dot{\alpha}}$, $m_{\dot{\beta}}$ Non-dimensional, equivalent constant strip, pitching-moment damping derivatives for motion in normal translation, pitch, control-surface rotation, respectively

Pitching moment measured about leading edge of local strip, positive nose up

h_β Non-dimensional, equivalent constant strip, hinge-moment stiffness derivative for motion in control-surface rotation

$h_{\dot{\beta}}$ Non-dimensional, equivalent constant strip hinge-moment damping derivative for motion in control surface rotation. Hinge moment positive direction control surface nose up

$(l_\theta)_f$ Non-dimensional, overall lift stiffness derivative for pitching motion about forward axis position $(= 0{\cdot}6789l_\alpha + 0{\cdot}0192l_z)$

$(l_{\dot{\theta}})_f$ Non-dimensional, overall lift damping derivative for pitching motion about forward axis position $(= -0{\cdot}0376l_{\dot{z}} + 0{\cdot}5115l_{\dot{\alpha}})$

$(m_\theta)_f$ Non-dimensional, overall moment stiffness derivative for pitching motion about forward axis position $(= -0{\cdot}05675l_z - 0{\cdot}1674l_\alpha - 0{\cdot}03763m_z + 0{\cdot}5115m_\alpha)$

$(m_{\dot{\theta}})_f$ Non-dimensional, overall moment damping derivative for pitching motion about forward axis position $(= -0{\cdot}0141l_{\dot{z}} - 0{\cdot}1027l_{\dot{\alpha}} - 0{\cdot}0518m_{\dot{z}} + 0{\cdot}4088m_{\dot{\alpha}})$

$(l_\theta)_r$ Non-dimensional, overall lift stiffness derivative for pitching motion about the rear axis position $(= -0{\cdot}6789l_\alpha - 0{\cdot}3862l_z)$

$(l_{\dot{\theta}})_r$ Non-dimensional, overall lift damping derivative for pitching motion about the rear axis position $(= -0{\cdot}3128l_{\dot{z}} + 0{\cdot}5115l_{\dot{\alpha}})$

$(m_\theta)_r$ Non-dimensional, overall moment stiffness derivative for pitching motion about rear axis position $(= 0{\cdot}0734l_z - 0{\cdot}1674l_\alpha - 0{\cdot}3128m_z + 0{\cdot}5115m_\alpha)$

$(m_{\dot{\theta}})_r$ Non-dimensional, overall moment damping derivative for pitching motion about rear axis position $(= 0{\cdot}0537l_{\dot{z}} - 0{\cdot}1027l_{\dot{\alpha}} - 0{\cdot}2591m_{\dot{z}} + 0{\cdot}4088m_{\dot{\alpha}})$

REFERENCES

No.	*Author*	*Title, etc.*
1	P. R. Guyett and J. K. Curran ..	Aerodynamic derivative measurements on a rectangular wing of aspect ratio 3·3. A.R.C. R. & M. 3171. March, 1958.
2	C. Scruton, L. Woodgate and A. J. Alexander	Measurements of the aerodynamic derivatives for swept wings of low aspect ratio describing pitching and plunging oscillations in incompressible flow. A.R.C. R. & M. 2925. October, 1953.
3	K. C. Wight	Measurements of two-dimensional derivatives on a wing-aileron-tab system with a 1541 section aerofoil. Part II—Direct tab and cross aileron-tab derivatives. A.R.C. R. & M. 3029. March, 1955.
4	W. D. T. Hicks	An electronic instrument for the accurate measurement of the frequency of structural oscillations. A.R.C. 17,920. January, 1955.
5	H. Templeton	The technique of flutter calculations. A.R.C. C.P.172. April, 1953.
6	W. P. Jones	Wind tunnel interference effects on the values of experimentally determined derivative coefficients for oscillating aerofoils. A.R.C. R. & M. 1912. August, 1943.
7	W. E. Acum and H. C. Garner ..	Approximate wall corrections for an oscillating swept wing in a wind tunnel of closed circular section. A.R.C. C.P.184. January, 1954.
8	Doris E. Lehrian	Calculation of flutter derivatives for wings of general planform. A.R.C. R. & M. 2961. January, 1954.
9	I. Minhinnick	Subsonic aerodynamic flutter derivatives for wings and control surfaces (compressible and incompressible flow). A.R.C. 14,228. July, 1950. (Addendum and Corrigendum in 14,855).
10	H. R. Lawrence and E. H. Gerber	The aerodynamic forces on low aspect ratio wings oscillating in an incompressible flow. *J. Ae. Sci.* Vol. 19. No. 11. November, 1952.

APPENDIX

Estimates of the Corrections to the Measured Derivatives Arising from Rig Deformation

The deformation was not measured during the tests but from observation it was clear that the primary mode was twist of the root frame. This mode was therefore chosen, together with displacement at the root transducer(s), and the prescribed wing or control motion, to define a system with a limited number of degrees of freedom. Lagrangian equations were then set up and solved to establish the amplitudes in each degree of freedom. From these results the corrections to the measured derivatives were found. The procedure for wing pitch about the forward axis position is described below.

The wing and support system are shown in Fig. 7.

The co-ordinates are

θ Angle of pitch, positive wing nose up,

ϕ Angle of roll, positive wing tip down,

z Displacement of the wing in normal translation, positive downwards.

Coefficients in the Lagrangian equations were obtained as follows:

Inertia coefficients: these were found directly from measurements of the weight of the wing, support and excitation systems.

Stiffness coefficients: the stiffness forces arose from the displacement of the inertia balancing springs, the spring bearings in the system, and the twist of the root frame. For convenience, the transducer coupling the root frame to earth was also treated as a spring.

Generalised force coefficients:

(*a*) *Excitation forces*: the exciter provided a force of known amplitude and phase angle in relation to the displacement of the cantilever strip attached to the wing; thus the excitation force,

$$F = (F' + iF'')e^{i\omega t}$$

where F' and F'' are, respectively, the in-phase and in-quadrature components of force. Now the displacement of the exciter rod $= a_1\theta + b_1\phi + z$, where a_1 and b_1 are the distances of the exciter rod behind the pitch axis, and above the roll axis, respectively. Hence the generalised forces are:

$$F_\theta = Fa_1$$
$$F_\phi = Fb_1$$
$$F_z = F.$$

(*b*) *Aerodynamic forces*: approximations to the aerodynamic forces acting in the chosen modes arising from the pitching motion were found from the uncorrected derivatives and an assumed position for the spanwise centre of pressure. The remaining forces, lift, pitching moment and rolling moment due to translation and roll, were ignored in order to simplify the analysis*. Thus the generalised forces may be written:

$$Q_\theta = G(m_\theta + ivm_{\dot\theta})\theta,$$
$$Q_\phi = (C_\phi + iB_\phi)\theta,$$
$$Q_z = (C_z + iB_z)\theta,$$

where G, C_ϕ, C_z, B_z are known, and m_θ and $m_{\dot\theta}$ are the required, corrected, pitching-moment derivatives.

*It was later shown that for the calculated amplitudes the aerodynamic forces arising from the motion in translation and roll were negligible in comparison with the forces due to pitch.

Equations of motion: the equation of motion in the θ co-ordinate is, neglecting structural damping

$$A_{11}\ddot{\theta} + A_{12}\ddot{\phi} + A_{13}\ddot{z} + E_{11}\theta + E_{12}\phi + E_{13}z = F_\theta + Q_\theta, \quad (1)$$

where A_{11} is the direct inertia term, E_{11} the direct stiffness term, and so on. Corresponding equations are obtained for motion in ϕ and z, giving equations (2) and (3).

Let $\theta = \bar{\theta}e^{i\omega t}$, $\phi = \bar{\phi}e^{i\omega t}$, etc., where $\bar{\alpha}$, $\bar{\phi}$, $\bar{z}$ are the complex amplitudes in pitch, roll and translation, such that $\bar{\theta} = \bar{\theta}' + i\bar{\theta}''$, etc., and $\bar{\theta}'$, $\bar{\theta}''$ are the components of $\bar{\theta}$ in phase and in quadrature, respectively, with the displacement of the cantilever strip. Hence $\ddot{\theta} = -\omega^2\bar{\theta}e^{i\omega t}$, etc., where ω is the circular frequency of oscillation.

Displacement of Cantilever Strip.

The cantilever strip was attached to the channel supporting the wing and its displacement, x, comprised components of motion in each mode. Thus

$$x = a_2\theta + b_2\phi + z, \text{ and } \bar{x} = a_2\bar{\theta} + b_2\bar{\phi} + \bar{z} \quad (4)$$

The displacement of the cantilever strip provided the reference phase angle and its amplitude was always made equal to its still-air value; thus $\bar{x}$ was a real, known quantity.

Solution.

Equations (2), (3) and (4) enable the absolute values of $\bar{\theta}$, $\bar{\phi}$, and $\bar{z}$ to be found. In each case the calculated value of $\bar{z}$ agreed closely with the known displacement at the root transducer, and thus served to check the results. The pitching-moment derivatives m_θ and $m_{\dot{\theta}}$ were then given by equation (1).

By taking moments about the cross-spring axis coupling the rectangular root frame to earth, a further equation was obtained establishing values for the corrected lift derivatives l_θ and $l_{\dot{\theta}}$.

Results obtained in this way could be used to give more accurate values for the coefficients Q_ϕ and Q_z in equations (2) and (3) and hence more accurate values for $\bar{\phi}$ and $\bar{z}$. In practice the corrections to the derivatives were so small that it was not worth-while following this iterative process.

Tables.

The results given are not corrected for wind-tunnel interference. The test Reynolds number varied between $0{\cdot}35 \times 10^6$ at the frequency parameter $1{\cdot}1$, and $1{\cdot}4 \times 10^6$ at frequency parameter $0{\cdot}27$. (Both Reynolds number and frequency parameter based on wing mean chord).

TABLE 1

Results for Wing Pitch about the Forward Axis Position

Wing mean angle of incidence = 0°. Amplitude in pitch = 3·54 degrees.

$(l_\theta)_f$

v_m	Aileron setting (degrees)			
	0	5	10	15
0·312	0·906	0·940	0·923	0·894
0·364	0·891	0·960	0·970	0·908
0·437	0·877	0·990	0·954	0·917
0·546	0·878	1·003	1·002	0·969
0·728	0·904	0·980	0·942	0·930

$(l_{\dot\theta})_f$

v_m	Aileron setting (degrees)			
	0	5	10	15
0·312	0·537	0·616	0·581	0·473
0·364	0·546	0·597	0·558	0·491
0·437	0·570	0·579	0·533	0·538
0·546	0·531	0·579	0·485	0·611
0·728	0·532	0·608	0·467	0·572

$(-m_\theta)_f$

v_m	Aileron setting (degrees)			
	0	5	10	15
0·312	0·425	0·451	0·458	0·452
0·364	0·418	0·457	0·480	0·454
0·437	0·414	0·472	0·476	0·458
0·546	0·418	0·476	0·492	0·473
0·728	0·435	0·470	0·469	0·470

TABLE 1—*continued*

$(-m_{\dot{\theta}})_f$

ν_m	Aileron setting (degrees)			
	0	5	10	15
0·312	0·339	0·377	0·356	0·314
0·364	0·344	0·366	0·348	0·322
0·437	0·354	0·354	0·339	0·335
0·546	0·335	0·362	0·321	0·363
0·728	0·339	0·362	0·308	0·352

TABLE 2

Results for Wing Pitch about the Rear Axis Position

Amplitude in pitch = 2·78 degrees. Wing mean angle of incidence = 0°.

$(l_\theta)_r$

ν_m	Aileron setting (degrees)			
	0	5	10	15
0·312	0·886	0·945	0·986	0·919
0·364	0·892	0·942	0·949	0·916
0·437	0·888	0·921	0·943	0·896
0·546	0·893	0·900	0·922	0·891
0·728	0·887	0·911	0·940	0·902

$(l_{\dot{\theta}})_r$

ν_m	Aileron setting (degrees)			
	0	5	10	15
0·312	0·241	0·230	0·167	0·131
0·364	0·251	0·244	0·186	0·151
0·437	0·249	0·243	0·216	0·167
0·546	0·263	0·247	0·260	0·198
0·728	0·286	0·260	0·319	0·245

TABLE 2—*continued*

$(-m_{\theta})_r$

ν_m	Aileron setting (degrees)			
	0	5	10	15
0·312	0·413	0·440	0·468	0·430
0·364	0·415	0·438	0·451	0·429
0·437	0·414	0·429	0·448	0·417
0·546	0·413	0·418	0·439	0·414
0·728	0·413	0·426	0·447	0·421

$(-m_{\dot{\theta}})_r$

ν_m	Aileron setting (degrees)			
	0	5	10	15
0·312	0·201	0·196	0·158	0·133
0·364	0·208	0·204	0·169	0·145
0·437	0·210	0·203	0·184	0·154
0·546	0·222	0·204	0·210	0·175
0·728	0·236	0·213	0·246	0·205

TABLE 3

Results for Control-Surface Oscillations with Wing Fixed

Wing angle of incidence = 0°.

	Mean aileron angle (degrees)							
	0 without transition wires		0 with transition wires		5 with transition wires		10 with transition wires	
β degrees	4·24	8·65	4·30	8·74	4·30	8·42	4·18	8·42
ν_m	l_β							
0·273	0·902	—	0·850	—	0·983	—	0·987	—
0·312	0·891	0·919	0·865	0·889	0·969	0·880	1·001	0·983
0·364	0·898	0·926	0·861	0·895	0·932	0·889	0·989	0·993
0·437	0·897	0·933	0·856	0·887	0·902	0·881	1·004	0·990
0·546	—	0·925	—	0·891	—	0·872	—	0·992
0·728	—	0·909	—	0·910	—	0·865	—	0·946
1·092	—	—	—	0·903	—	0·839	—	0·952
	$l_{\dot\beta}$							
0·273	0·227	—	0·122	—	0·164	—	0·140	—
0·312	0·222	0·137	0·197	0·160	0·183	0·176	0·193	0·145
0·364	0·211	0·154	0·201	0·188	0·200	0·173	0·241	0·181
0·437	0·167	0·184	0·225	0·175	0·199	0·167	0·232	0·197
0·546	—	0·165	—	0·194	—	0·196	—	0·204
0·728	—	0·161	—	0·180	—	0·195	—	0·247
1·092	—	—	—	0·178	—	0·155	—	0·238
	$-(0\cdot5115m_\beta-0\cdot1674l_\beta)$							
0·273	0·431	—	0·407	—	0·473	—	0·473	—
0·312	0·427	0·440	0·415	0·426	0·467	0·420	0·482	0·473
0·364	0·430	0·443	0·413	0·431	0·447	0·425	0·476	0·479
0·437	0·431	0·448	0·413	0·428	0·432	0·423	0·485	0·477
0·546	—	0·442	—	0·428	—	0·418	—	0·479
0·728	—	0·437	—	0·439	—	0·414	—	0·456
1·092	—	—	—	0·437	—	0·405	—	0·462
	$-(0\cdot4088m_{\dot\beta}-0\cdot1027l_{\dot\beta})$							
0·273	0·1012	—	0·0696	—	0·0822	—	0·0740	—
0·312	0·0996	0·0674	0·0888	0·0772	0·0868	0·0822	0·1103	0·0759
0·364	0·0936	0·0748	0·0903	0·0906	0·0947	0·0798	0·1175	0·0867
0·437	0·0786	0·0879	0·0996	0·0860	0·0943	0·0809	0·1098	0·0923
0·546	—	0·0779	—	0·0901	—	0·0898	—	0·0930
0·728	—	0·0787	—	0·0863	—	0·0888	—	0·1095
1·092	—	—	—	0·0841	—	0·0738	—	0·1035

TABLE 3—*continued*

Wing angle of incidence = 0°.

	Mean aileron angle (degrees)							
	0 without transition wires		0 with transition wires		5 with transition wires		10 with transition wires	
β degrees	4·24	8·65	4·30	8·74	4·30	8·42	4·18	8·42
ν_m	(h_β)							
0·273	0·0076	—	0·0077	—	0·0092	—	0·0098	—
0·312	0·0071	0·0088	0·0076	0·0087	0·0089	0·0086	0·0092	0·0093
0·364	0·0070	0·0083	0·0079	0·0087	0·0094	0·0085	0·0096	0·0092
0·437	0·0070	0·0081	0·0080	0·0087	0·0091	0·0077	0·0091	0·0091
0·546	—	0·0076	—	0·0090	—	0·0082	—	0·0099
0·728	—	0·0065	—	0·0089	—	0·0077	—	0·0089
1·092	—	—	—	0·0091	—	0·0072	—	0·0096
	$(-h_{\dot{\beta}})$							
0·273	0·0112	—	0·0124	—	0·0131	—	0·0152	—
0·312	0·0115	0·0117	0·0117	0·0120	0·0133	0·0125	0·0147	0·0136
0·364	0·0119	0·0116	0·0119	0·0115	0·0137	0·0121	0·0149	0·0131
0·437	0·0116	0·0109	0·0122	0·0113	0·0140	0·0120	0·0134	0·0137
0·546	—	0·0114	—	0·0109	—	0·0124	—	0·0140
0·728	—	0·0109	—	0·0113	—	0·0120	—	0·0143
1·092	—	—	—	0·0109	—	0·0118	—	0·0159

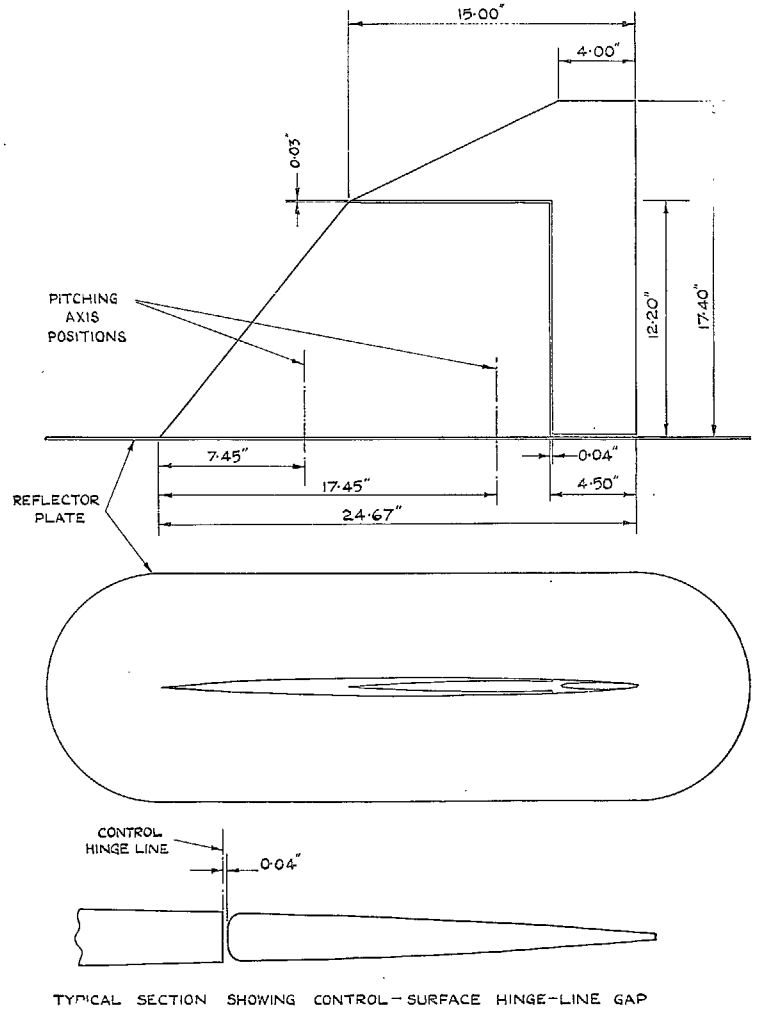

FIG. 1. Wing and control-surface dimensions.

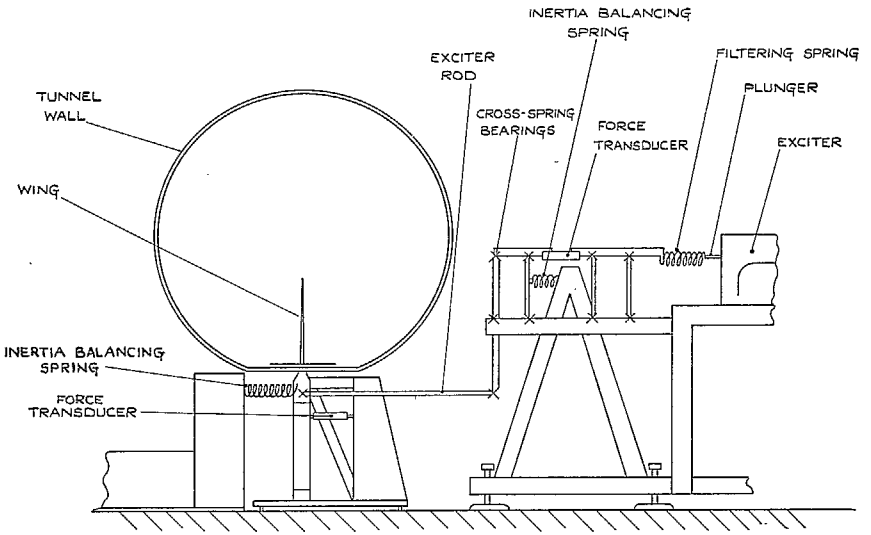

FIG. 2. Diagrammatic arrangement of wing and equipment in wind-tunnel working section.

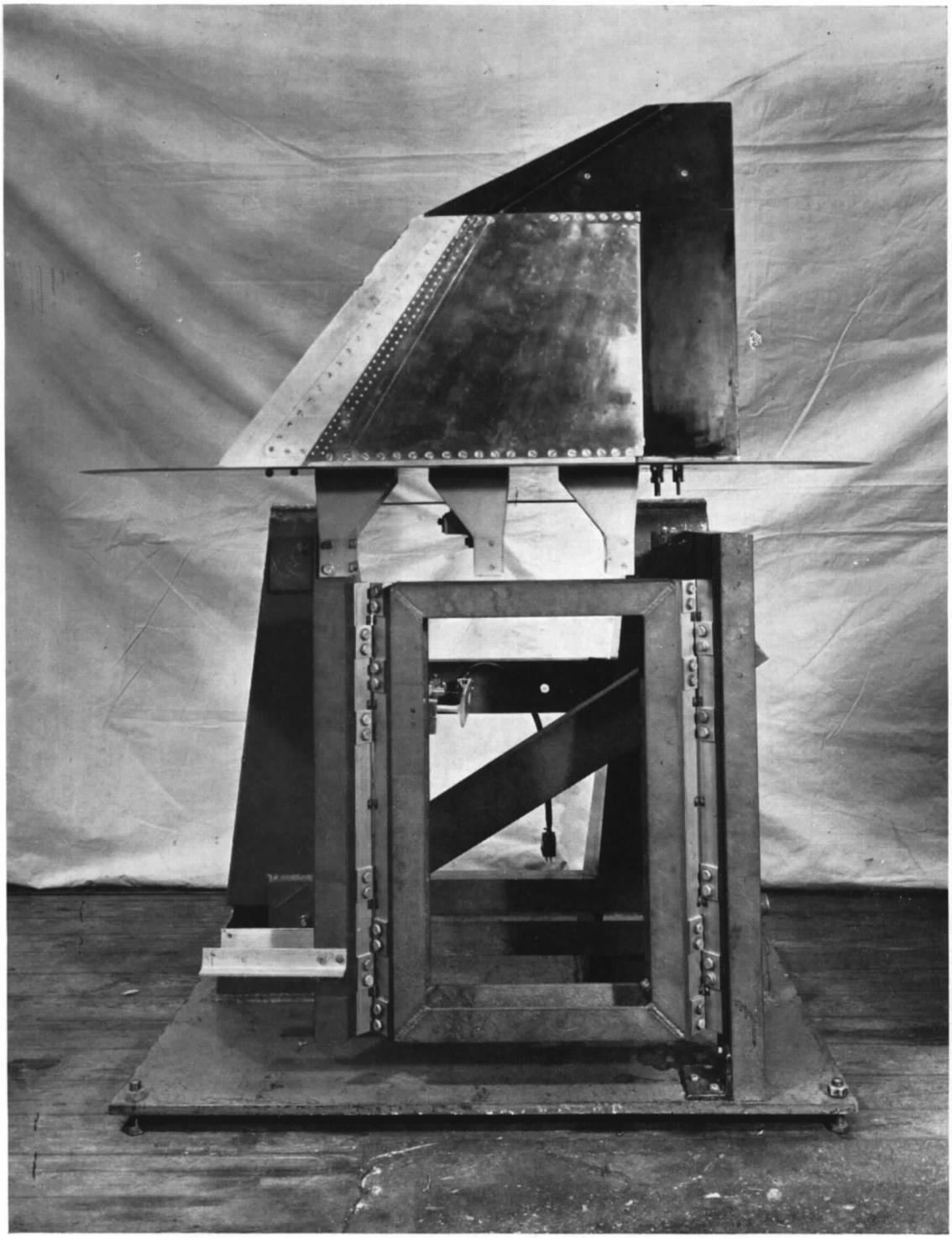

FIG. 3. Wing and root support frame.

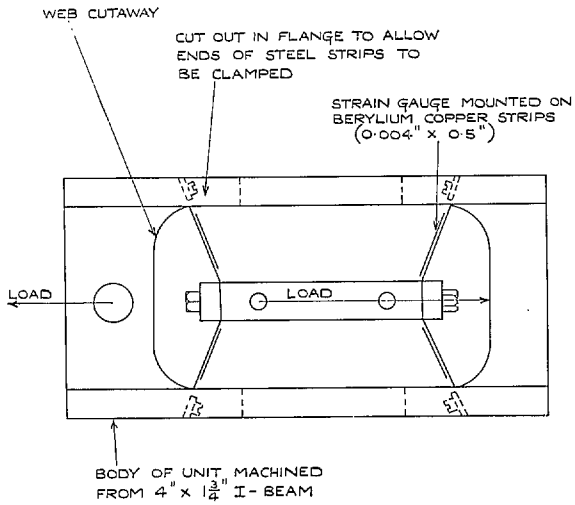

FIG. 4. Force-measuring transducer.

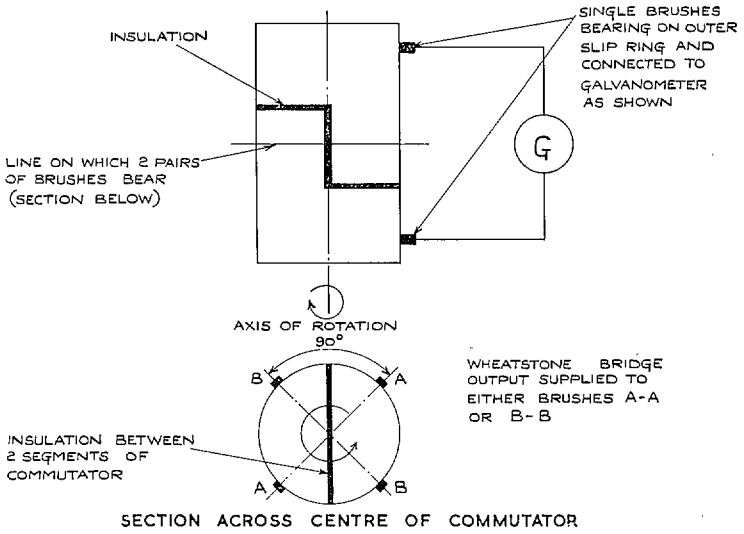

FIG. 5. The commutator and brush arrangement.

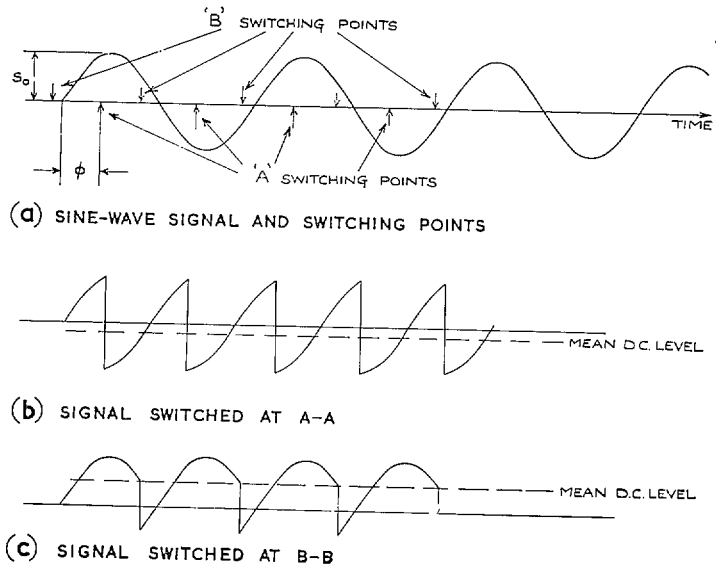

FIGS. 6a to c. Gauge output signal and switching.

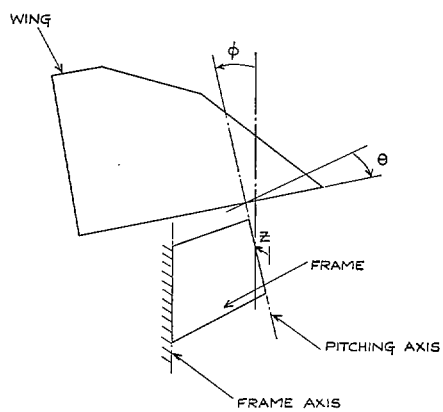

FIG. 7. Wing displacements: forward axis position.

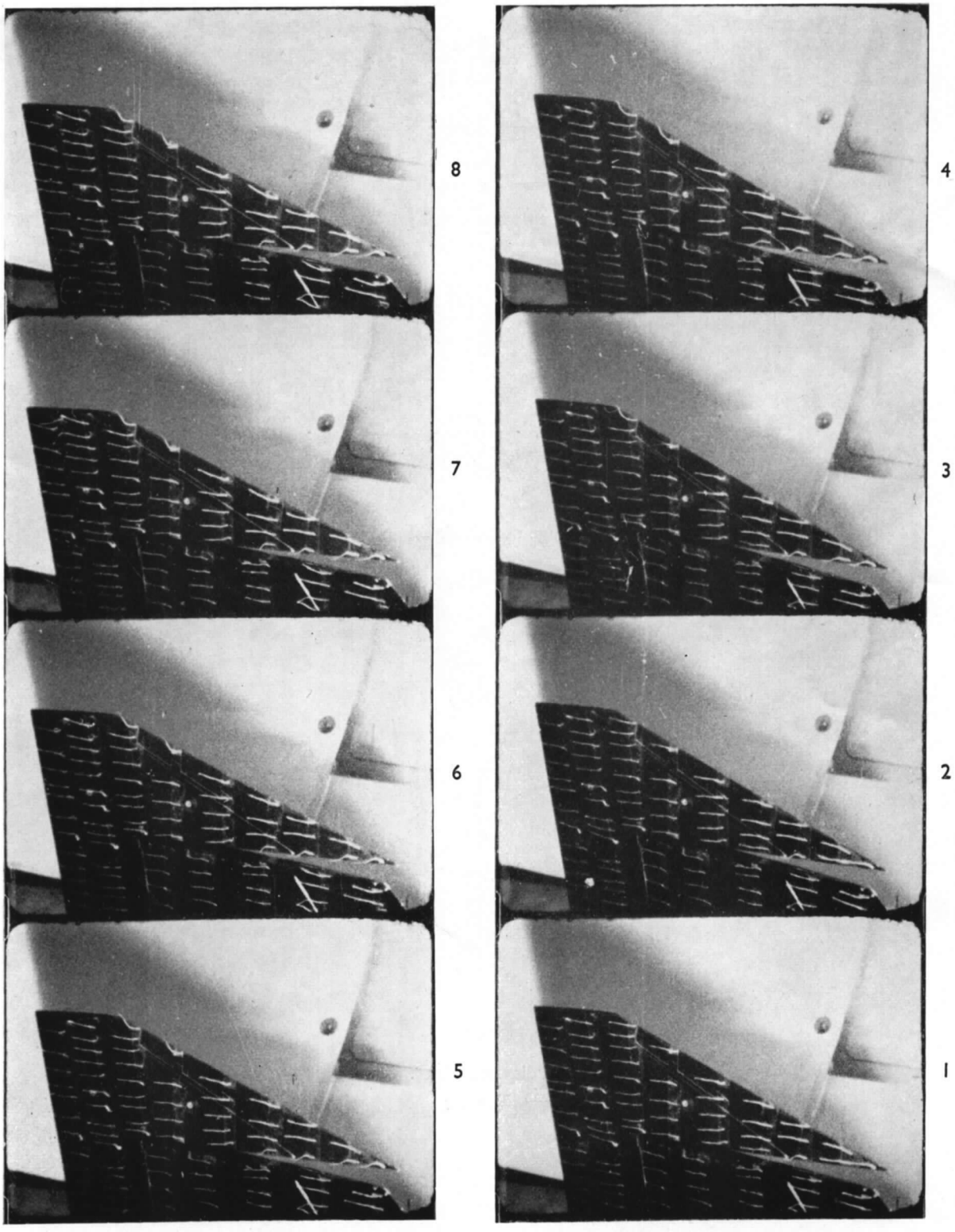

FIG. 8. Cine camera pictures of wing oscillation.

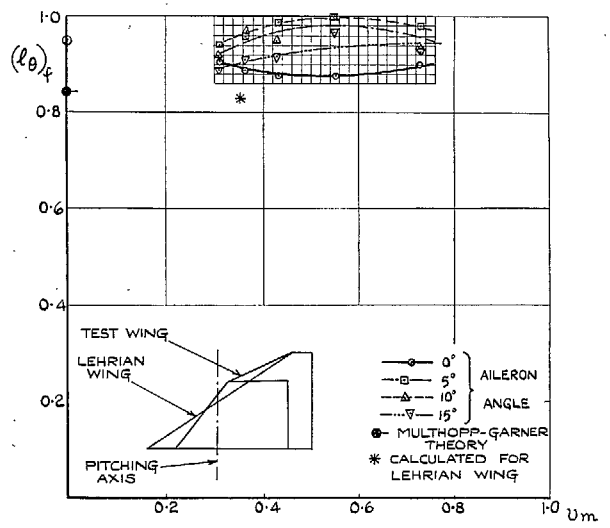

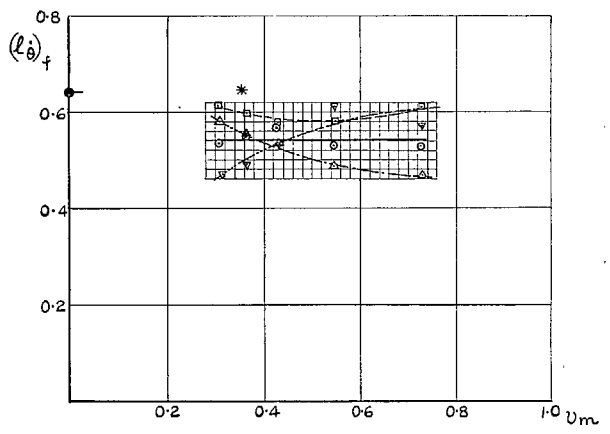

FIG. 9. Variation of $(l_\theta)_f$ and $(l_{\dot\theta})_f$ with v_m.

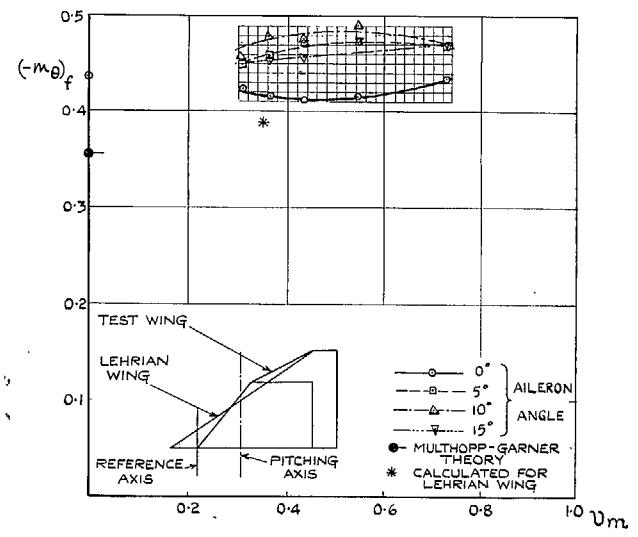

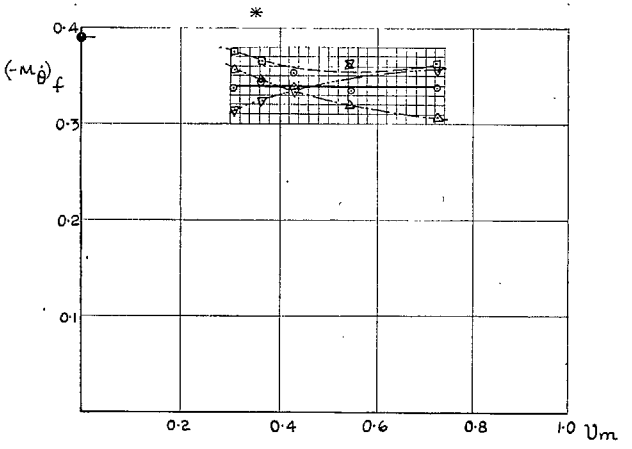

FIG. 10. Variation of $(-m_\theta)_f$ and $(-m_{\dot\theta})_f$ with v_m.

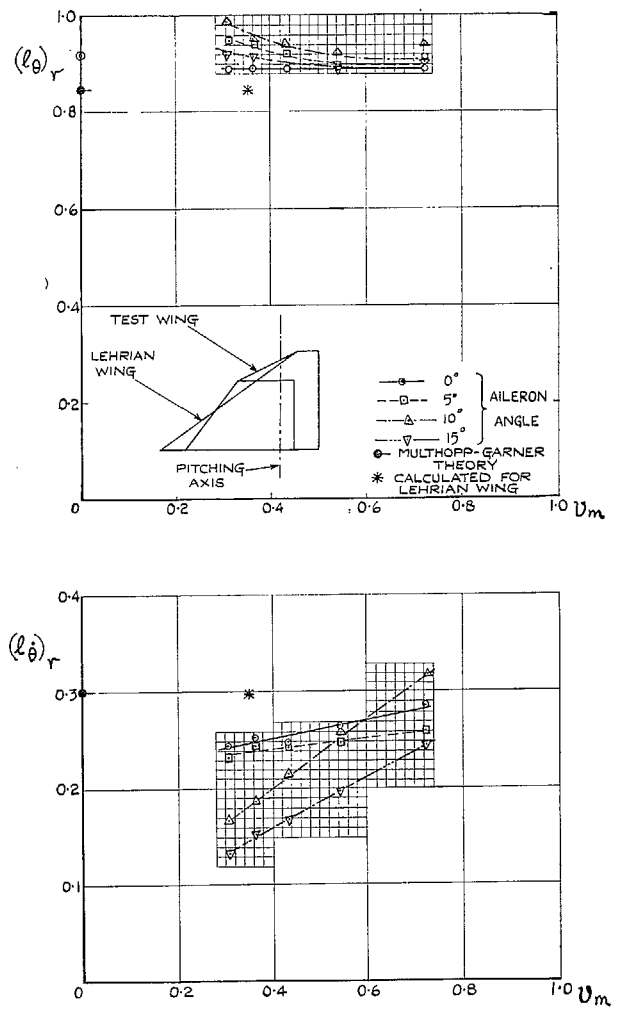

FIG. 11. Variation of $(l_\theta)_r$ and $(l_{\dot\theta})_r$ with ν_m.

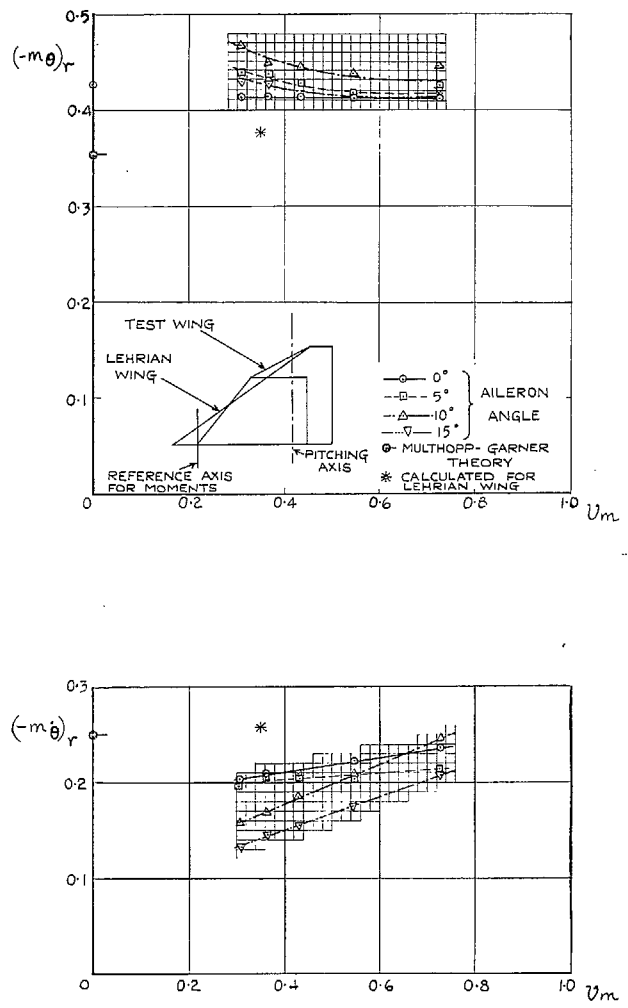

FIG. 12. Variation of $(-m_\theta)_r$ and $(-m_{\dot\theta})_r$ with ν_m.

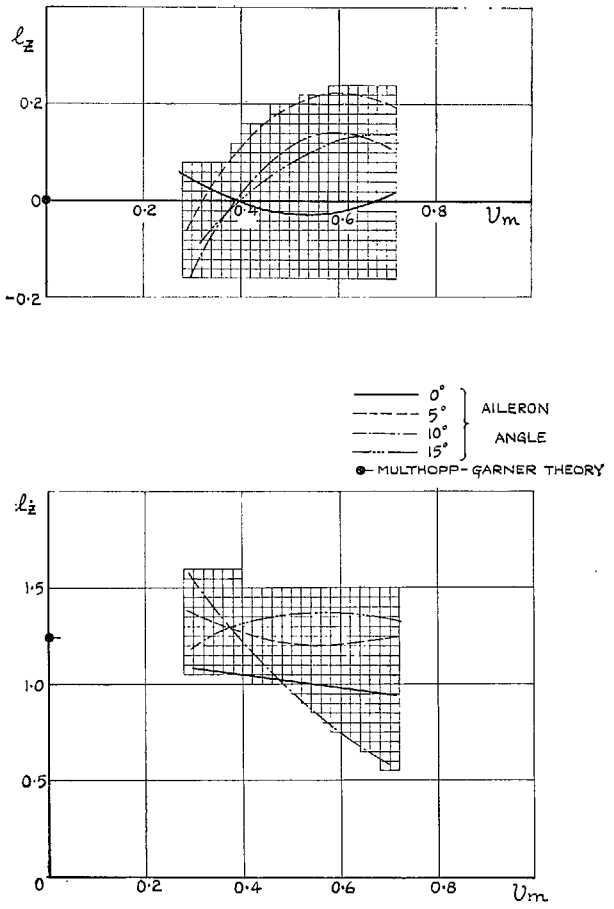

FIG. 13. Variation of l_z and $l_{\dot{z}}$ with v_m.

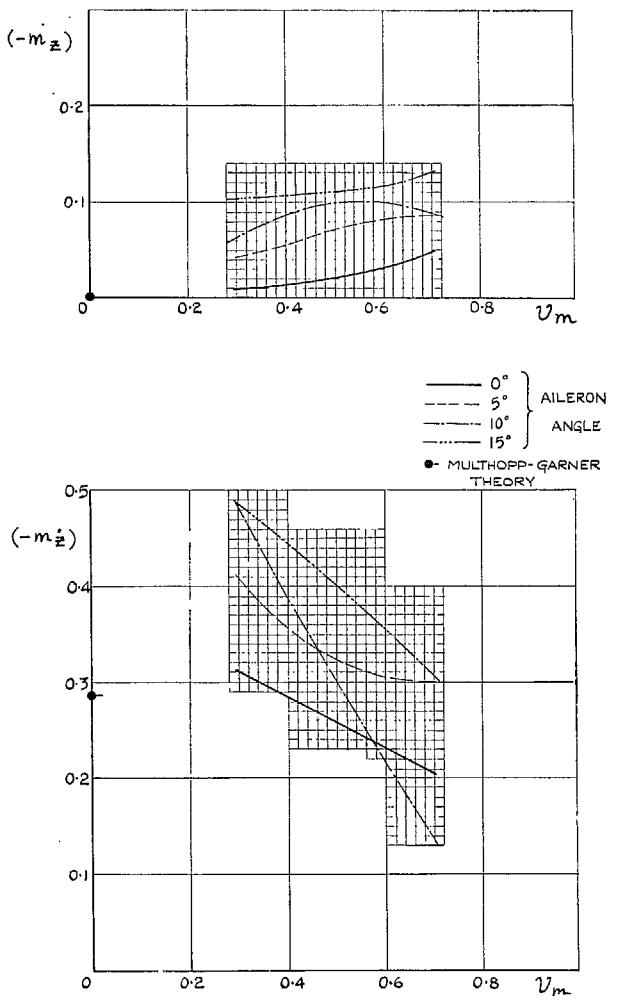

FIG. 14. Variation of $(-m_z)$ and $-m_{\dot{z}})$ with v_m.

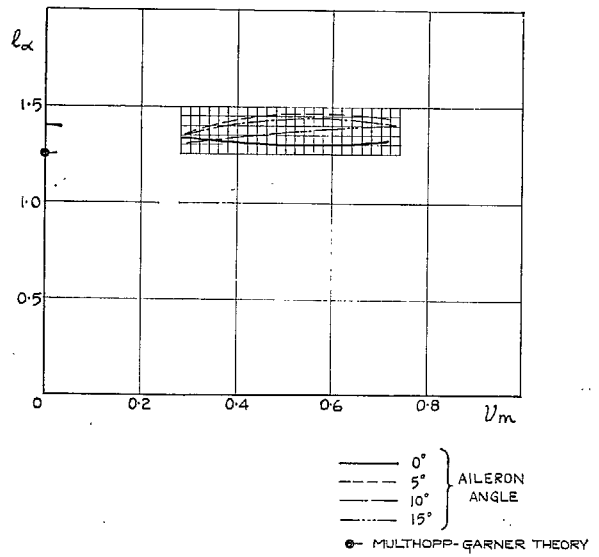

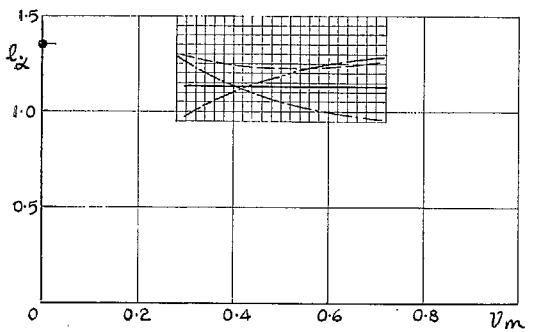

FIG. 15. Variation of l_α and $l_{\dot\alpha}$ with v_m.

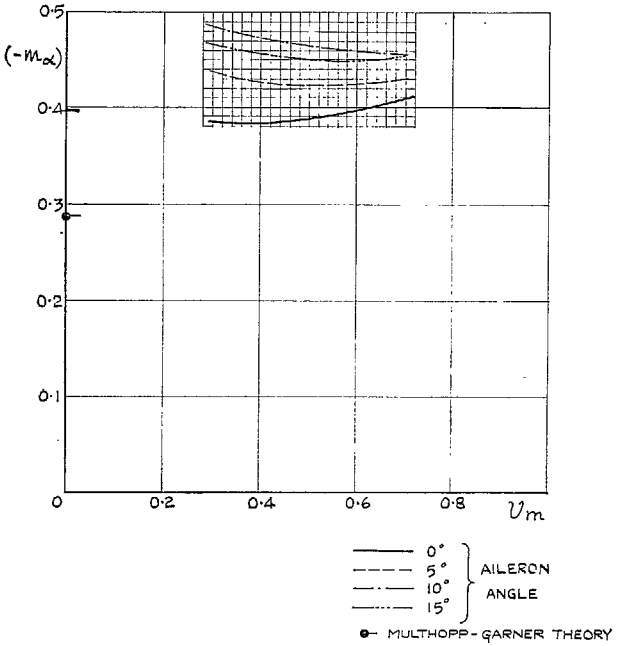

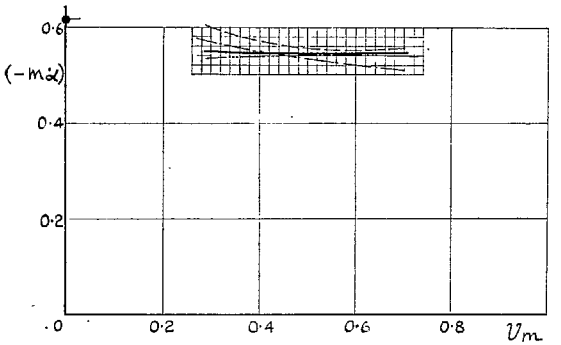

FIG. 16. Variation of $(-m_\alpha)$ and $-m_{\dot\alpha})$ with v_m.

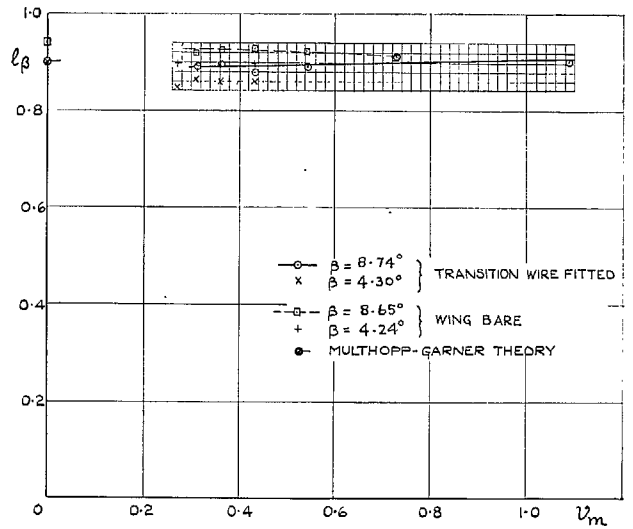

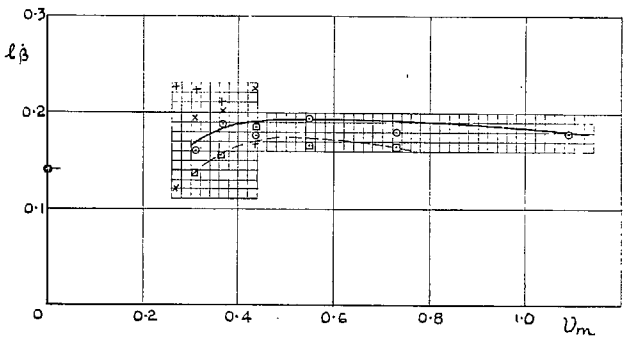

FIG. 17. Variation of l_β and $l_{\dot\beta}$ with ν_m: mean aileron angle 0°.

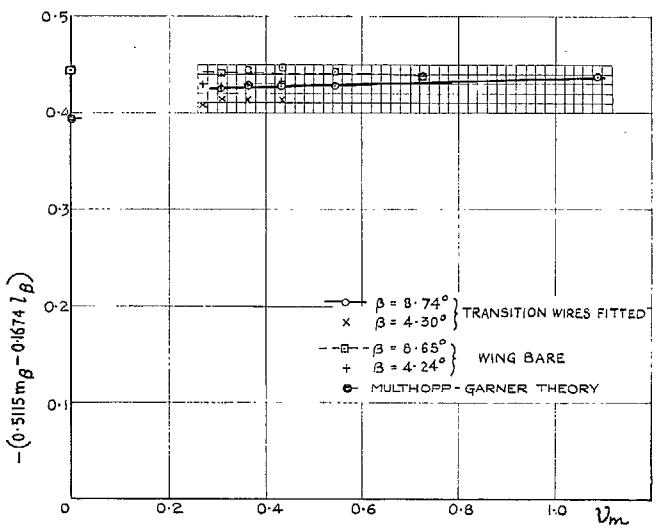

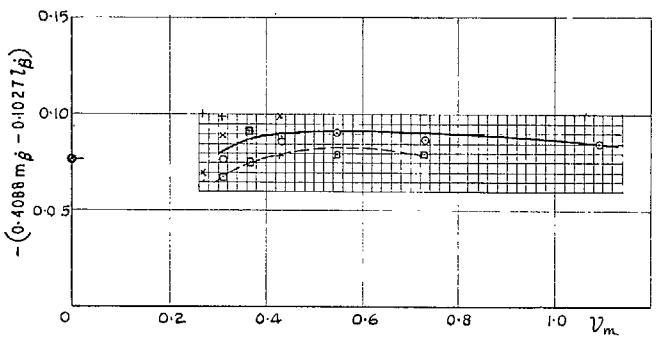

FIG 18. Variation of $-(0{\cdot}5115m_\beta - 0{\cdot}1674l_\beta)$ and $-(0{\cdot}4088m_{\dot\beta} - 0{\cdot}1027l_{\dot\beta})$ with ν_m: mean aileron angle 0°.

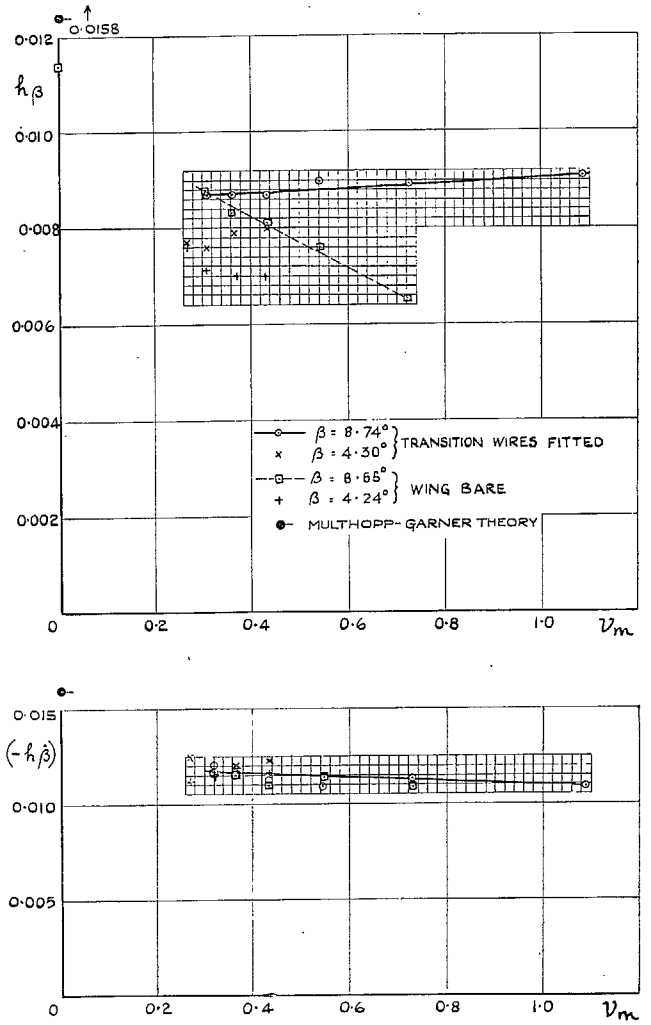

FIG. 19. Variation of h_β and $(-h_{\dot\beta})$ with v_m: mean aileron angle 0°.

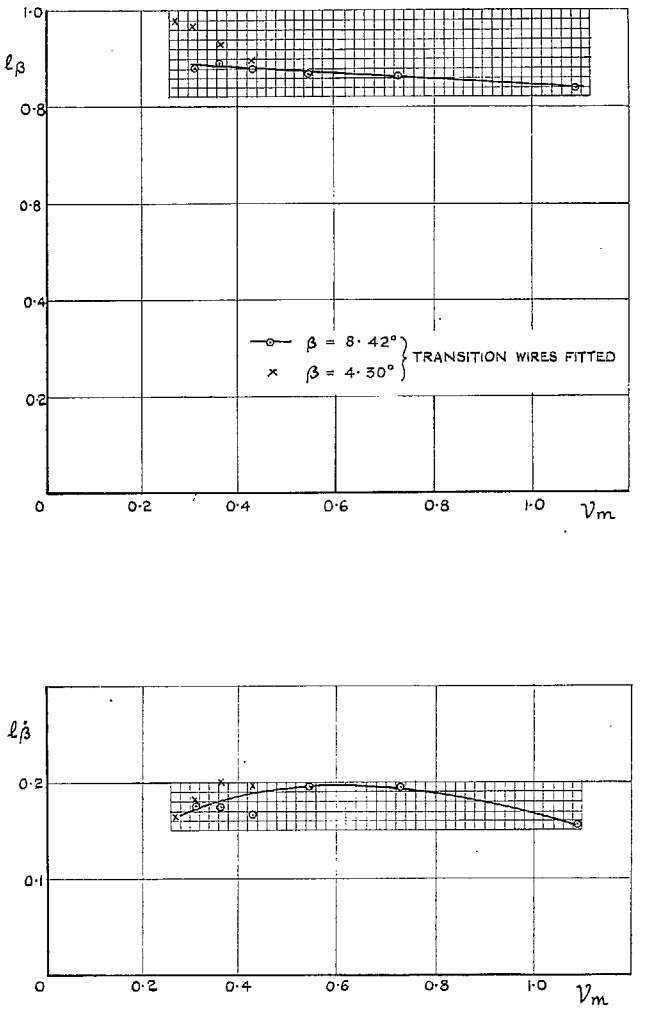

FIG. 20. Variation of l_β and $l_{\dot\beta}$ with v_m: mean aileron angle 5°.

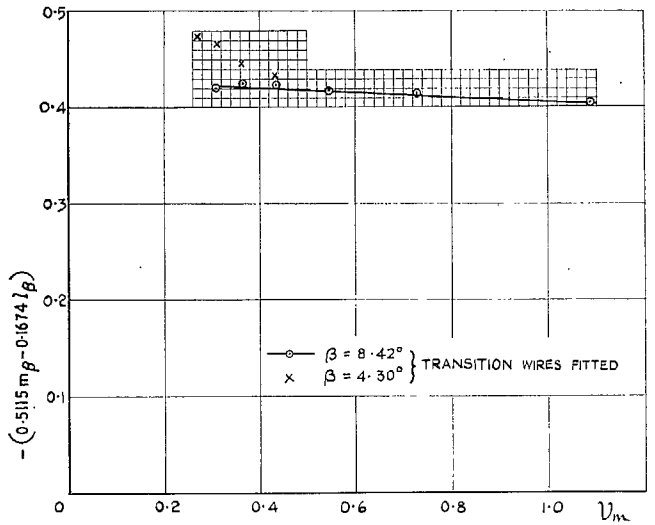

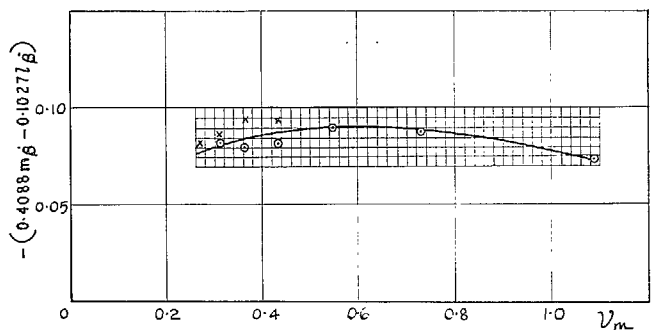

FIG. 21. Variation of $-(0{\cdot}5115m_\beta - 0{\cdot}1674l_\beta)$ and $-(0{\cdot}4088m_{\dot\beta} - 0{\cdot}1027l_{\dot\beta})$ with ν_m: mean aileron angle 5°.

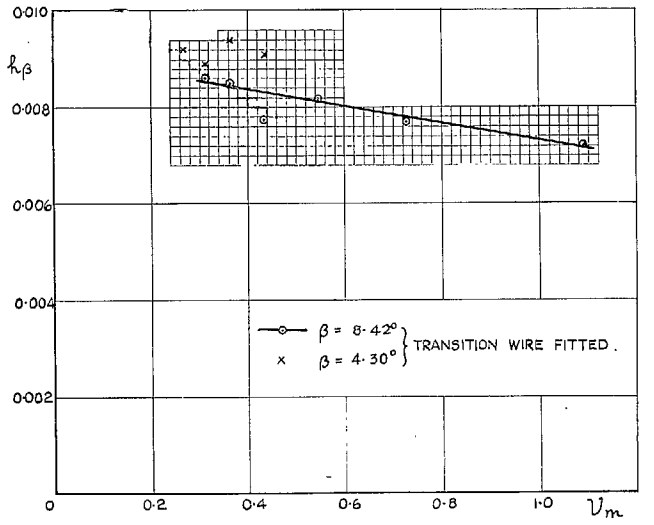

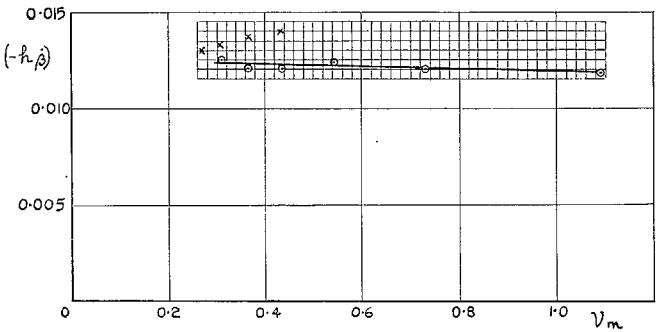

FIG. 22. Variation of h_β and $(-h_{\dot\beta})$ with ν_m: mean aileron angle 5°.

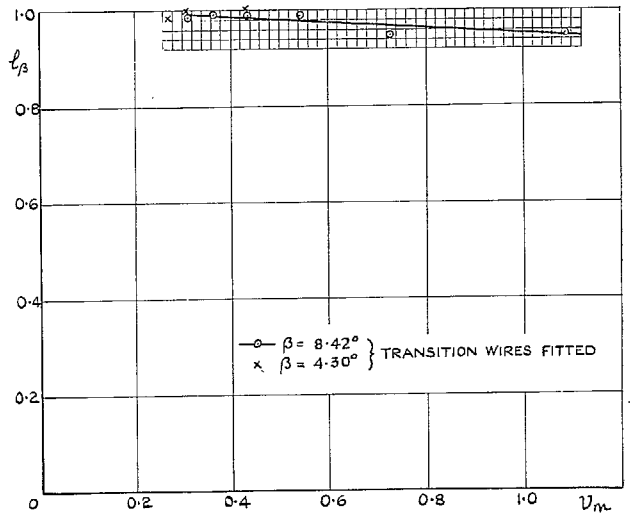

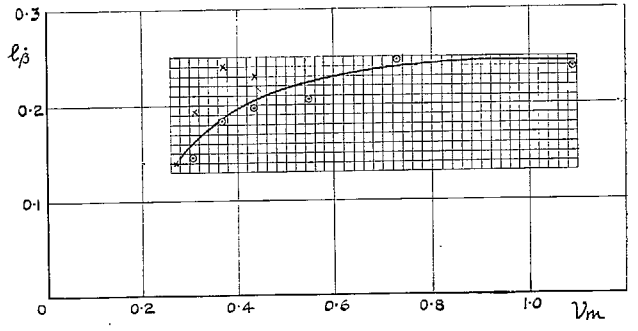

FIG. 23. Variation of l_β and $l_{\dot\beta}$ with v_m: mean aileron angle 10°.

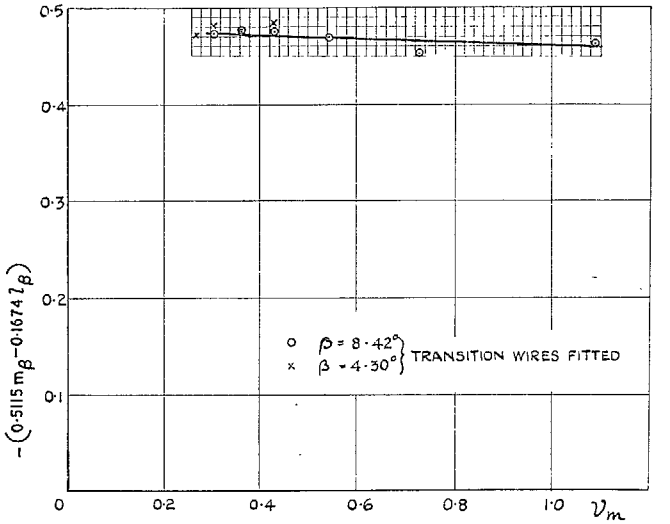

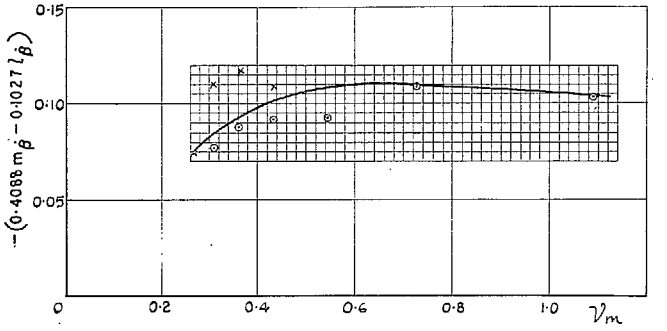

FIG. 24. Variation of $-(0{\cdot}5115m_\beta - 0{\cdot}1674l_\beta)$ and $-(0{\cdot}4088m_{\dot\beta} - 0{\cdot}1027l_{\dot\beta})$ with v_m: mean aileron angle 10°.

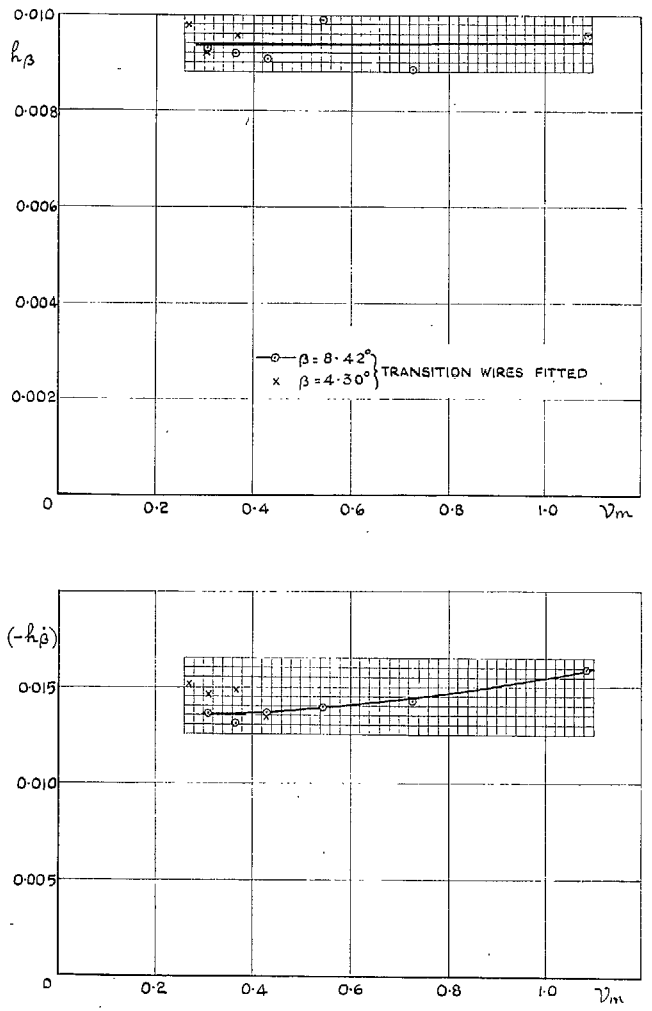

FIG. 25. Variation of h_β and $(-h_{\dot\beta})$ with v_m: mean aileron angle 10°.

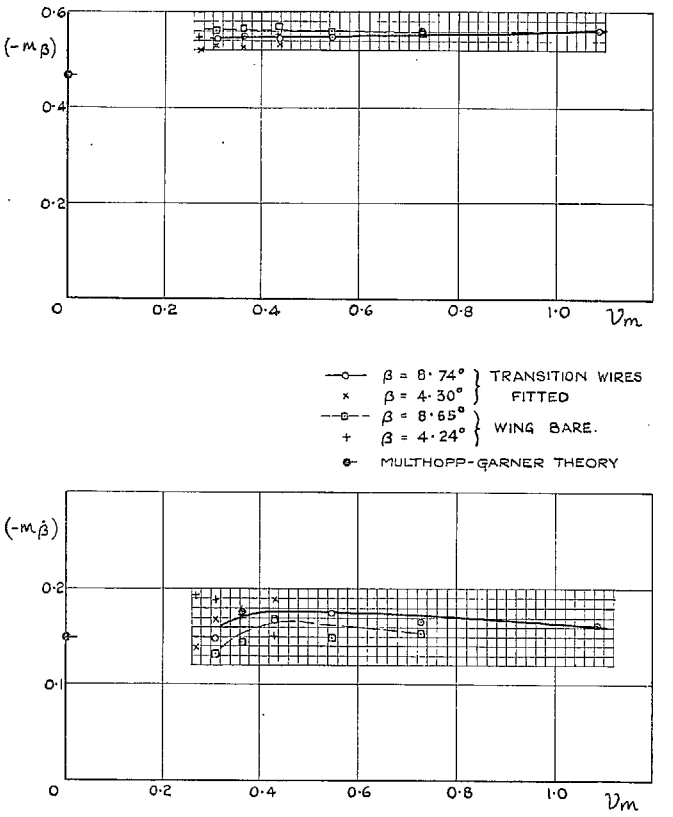

FIG. 26. Variation of $(-m_\beta)$ and $(-m_{\dot\beta})$ with v_m: mean aileron angle 0°.

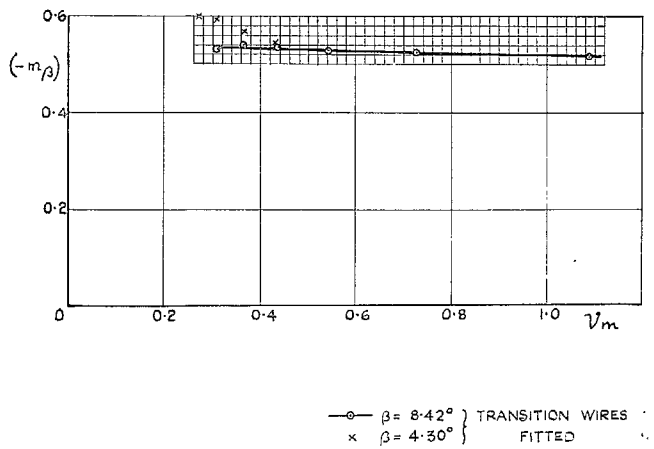

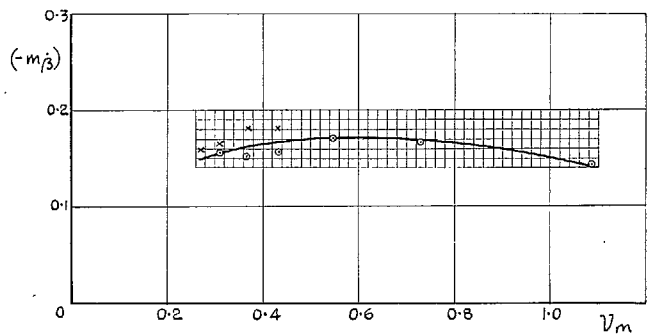

Fig. 27. Variation of $(-m_\beta)$ and $(-m_{\dot\beta})$ with v_m: mean aileron angle 5°.

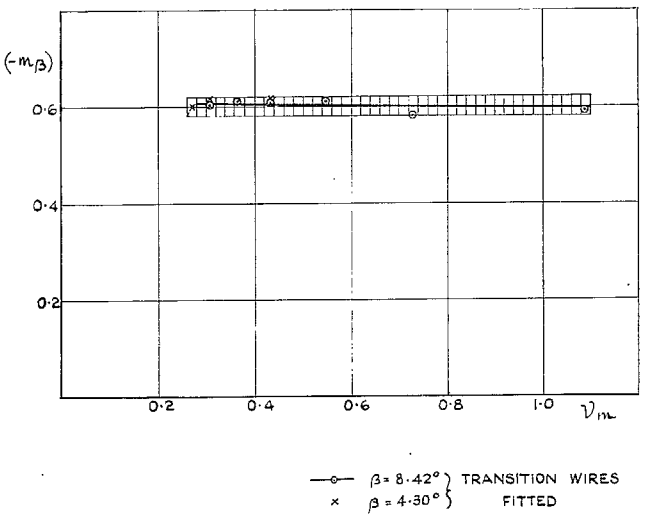

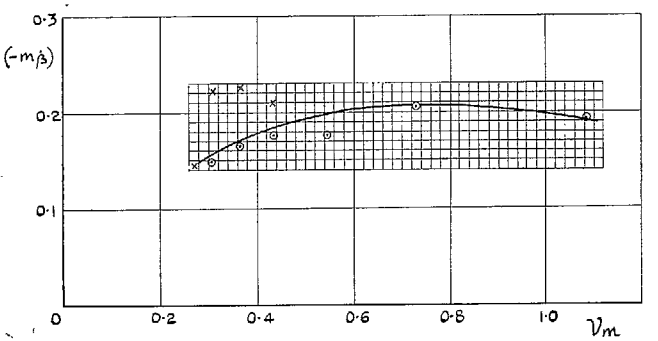

FIG. 28. Variation of $(-m_\beta)$ and $(-m_{\dot\beta})$ with v_m: mean aileron angle 10°.

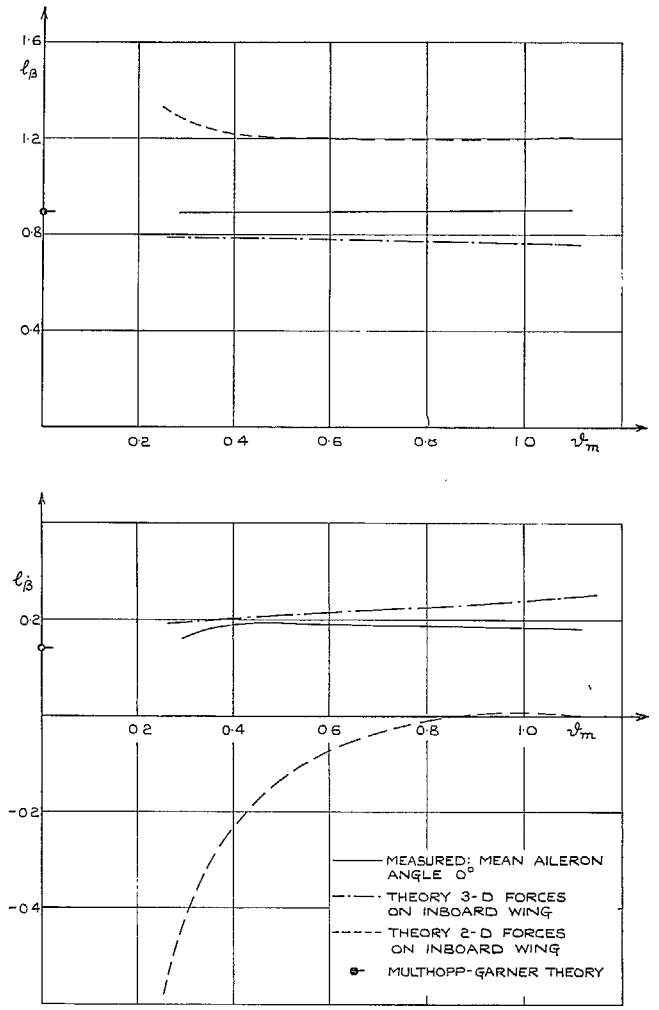

FIG. 29. Comparison of calculated and measured values for l_β and $l_{\dot\beta}$.

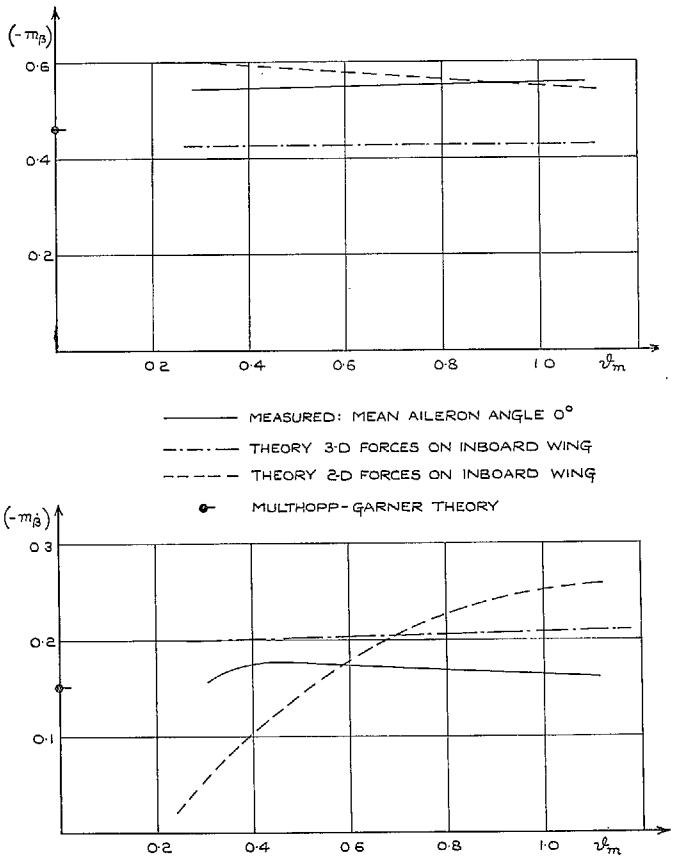

FIG. 30. Comparison of calculated and measured values for $(-m_\beta)$ and $(-m_{\dot\beta})$.

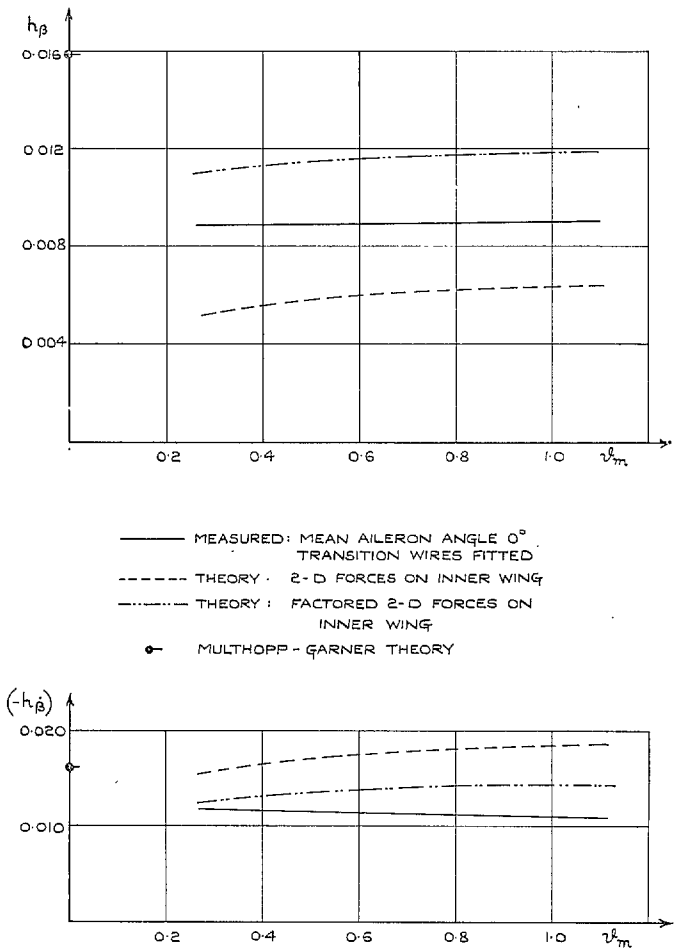

FIG. 31. Comparison of calculated and measured values for h_β and $(-h_{\dot\beta})$.

(86213) Wt. 64/1857 K.5 2/63 Hw.

Publications of the Aeronautical Research Council

ANNUAL TECHNICAL REPORTS OF THE AERONAUTICAL RESEARCH COUNCIL (BOUND VOLUMES)

1942 Vol. I. Aero and Hydrodynamics, Aerofoils, Airscrews, Engines. 75*s.* (post 2*s.* 9*d.*)
Vol. II. Noise, Parachutes, Stability and Control, Structures, Vibration, Wind Tunnels. 47*s.* 6*d.* (post 2*s.* 3*d.*)

1943 Vol. I. Aerodynamics, Aerofoils, Airscrews. 80*s.* (post 2*s.* 6*d.*)
Vol. II. Engines, Flutter, Materials, Parachutes, Performance, Stability and Control, Structures. 90*s.* (post 2*s.* 9*d.*)

1944 Vol. I. Aero and Hydrodynamics, Aerofoils, Aircraft, Airscrews, Controls. 84*s.* (post 3*s.*)
Vol. II. Flutter and Vibration, Materials, Miscellaneous, Navigation, Parachutes, Performance, Plates and Panels, Stability, Structures, Test Equipment, Wind Tunnels. 84*s.* (post 3*s.*)

1945 Vol. I. Aero and Hydrodynamics, Aerofoils. 130*s.* (post 3*s.* 6*d.*)
Vol. II. Aircraft, Airscrews, Controls. 130*s.* (post 3*s.* 6*d.*)
Vol. III. Flutter and Vibration, Instruments, Miscellaneous, Parachutes, Plates and Panels, Propulsion. 130*s.* (post 3*s.* 3*d.*)
Vol. IV. Stability, Structures, Wind Tunnels, Wind Tunnel Technique. 130*s.* (post 3*s.* 3*d.*)

1946 Vol. I. Accidents, Aerodynamics, Aerofoils and Hydrofoils. 168*s.* (post 3*s.* 9*d.*)
Vol. II. Airscrews, Cabin Cooling, Chemical Hazards, Controls, Flames, Flutter, Helicopters, Instruments and Instrumentation, Interference, Jets, Miscellaneous, Parachutes. 168*s.* (post 3*s.* 3*d.*)
Vol. III. Performance, Propulsion, Seaplanes, Stability, Structures, Wind Tunnels. 168*s.* (post 3*s.* 6*d.*)

1947 Vol. I. Aerodynamics, Aerofoils, Aircraft. 168*s.* (post 3*s.* 9*d.*)
Vol. II. Airscrews and Rotors, Controls, Flutter, Materials, Miscellaneous, Parachutes, Propulsion, Seaplanes, Stability, Structures, Take-off and Landing. 168*s.* (post 3*s.* 9*d.*)

1948 Vol. I. Aerodynamics, Aerofoils, Aircraft, Airscrews, Controls, Flutter and Vibration, Helicopters, Instruments, Propulsion, Seaplane, Stability, Structures, Wind Tunnels. 130*s.* (post 3*s.* 3*d.*)
Vol. II. Aerodynamics, Aerofoils, Aircraft, Airscrews, Controls, Flutter and Vibration, Helicopters, Instruments, Propulsion, Seaplane, Stability, Structures, Wind Tunnels. 110*s.* (post 3*s.* 3*d.*)

Special Volumes

Vol. I. Aero and Hydrodynamics, Aerofoils, Controls, Flutter, Kites, Parachutes, Performance, Propulsion, Stability. 126*s.* (post 3*s.*)
Vol. II. Aero and Hydrodynamics, Aerofoils, Airscrews, Controls, Flutter, Materials, Miscellaneous, Parachutes, Propulsion, Stability, Structures. 147*s.* (post 3*s.*)
Vol. III. Aero and Hydrodynamics, Aerofoils, Airscrews, Controls, Flutter, Kites, Miscellaneous, Parachutes, Propulsion, Seaplanes, Stability, Structures, Test Equipment. 189*s.* (post 3*s.* 9*d.*)

Reviews of the Aeronautical Research Council

1939–48 3*s.* (post 6*d.*) 1949–54 5*s.* (post 5*d.*)

Index to all Reports and Memoranda published in the Annual Technical Reports

1909–1947 R. & M. 2600 (out of print)

Indexes to the Reports and Memoranda of the Aeronautical Research Council

Between Nos. 2351–2449	R. & M. No. 2450	2*s.* (post 3*d.*)
Between Nos. 2451–2549	R. & M. No. 2550	2*s.* 6*d.* (post 3*d.*)
Between Nos. 2551–2649	R. & M. No. 2650	2*s.* 6*d.* (post 3*d.*)
Between Nos. 2651–2749	R. & M. No. 2750	2*s.* 6*d.* (post 3*d.*)
Between Nos. 2751–2849	R. & M. No. 2850	2*s.* 6*d.* (post 3*d.*)
Between Nos. 2851–2949	R. & M. No. 2950	3*s.* (post 3*d.*)
Between Nos. 2951–3049	R. & M. No. 3050	3*s.* 6*d.* (post 3*d.*)
Between Nos. 3051–3149	R. & M. No. 3150	3*s.* 6*d.* (post 3*d.*)

HER MAJESTY'S STATIONERY OFFICE

from the addresses overleaf

Printed and published by
HER MAJESTY'S STATIONERY OFFICE

To be purchased from
York House, Kingsway, London W.C.2
423 Oxford Street, London W.1
13A Castle Street, Edinburgh 2
109 St. Mary Street, Cardiff
39 King Street, Manchester 2
50 Fairfax Street, Bristol 1
35 Smallbrook, Ringway, Birmingham 5
80 Chichester Street, Belfast 1
or through any bookseller

Printed in England

S.O. Code No. 23-3307